The Importance of Soil Type Contrast in Modulating August Precipitation Distribution near the Edwards Plateau and Balcones Escarpment in Texas

Xiao-Ming Hu[1,2], Ming Xue[1,2], Renee A. McPherson[3,4]

[1]Center for Analysis and Prediction of Storms, and [2]School of Meteorology, University of Oklahoma, Norman, Oklahoma 73072, USA
[3]South Central Climate Science Center, and [4]Department of Geography and Environmental Sustainability, University of Oklahoma, Norman, Oklahoma 73072, USA

Submitted to *Journal of Geophysical Research*

1st submission on 4/26/2017
Revised on 8/17/2017 12:13 PM

Corresponding author address:
Dr. Xiao-Ming Hu
Center for Analysis and Prediction of Storms
University of Oklahoma
Norman, Oklahoma 73072, USA
Email: xhu@ou.edu
Phone: (405) 325- 5571

Abstract

The Balcones Escarpment in central Texas is a sloped region between the Edwards Plateau and the coastal plain. The metropolitan areas located along the Balcones Escarpment (e.g., San Antonio, Austin, and Dallas-Fort Worth) are prone to heavy rain and devastating flood events. While the associated hydrological issues of the Balcones Escarpment have been extensively studied, the meteorological impacts of the Edwards Plateau and Balcones Escarpment are not well understood. The indeterminate impacts of the thermal and dynamic effects of the Edwards Plateau on August climatological precipitation are investigated in this study using the multi-sensor Stage IV precipitation data, high-resolution dynamic downscaling, and short-term sensitivity simulations. Analysis results indicate that the total August precipitation east of the Balcones Escarpment is suppressed and precipitation over the eastern part of the Edwards Plateau is enhanced. Locally initiated moist convection in the afternoon contributes most to the total precipitation during August in the region. The dynamic downscaling output captures the spatial pattern of afternoon precipitation, which is well aligned with the simulated upward motions. The clay-based soil types that dominate the Edwards Plateau have great potential to retain soil moisture and limit latent heat fluxes, consequently leading to higher sensible heat flux than over the plain to the east. As a result, vertical motion is induced, triggering the afternoon moist convection over the Edwards Plateau under favorable conditions. In comparison, the sloping terrain plays a smaller role in triggering the convection. Short-term sensitivity simulations for a clear day confirm and further prove such a diagnosis.

Keywords: Stage IV precipitation data; WRF; spectral nudging; wilting point soil moisture

1. Introduction

The Balcones Escarpment in central Texas is a sloped region located between the Edwards Plateau and the relatively flat, sandy coastal plain [*Miller and White*, 1998; *Nielsen et al.*, 2016]. It contains several large urban areas, including San Antonio, Austin, and Dallas-Fort Worth (Fig. 1a). These cities, due to unique local topography and other factors (e.g., moist air advecting inland from the Gulf of Mexico), are particularly vulnerable to heavy rain and devastating flood events [*Ashley and Ashley*, 2008; *Saharia et al.*, 2017]. Such issues may become more of a concern in a changing climate [*Gleason et al.*, 2008; *Groisman and Knight*, 2008; *Zhang et al.*, 2013; *Shafter et al.*, 2014; *Steiner et al.*, 2014; *Westra et al.*, 2014; *Prein et al.*, 2017].

Issues associated with the hydrology of the Balcones Escarpment have been extensively studied, but the meteorological impacts of the Edwards Plateau and Balcones Escarpment have not been investigated until recently [*Hu and Xue*, 2016; *Nielsen et al.*, 2016]. In *Nielsen et al.* [2016], numerical sensitivity tests were conducted with and without the topography of the Edwards Plateau for three extreme precipitation events. Their modeling results showed that the intensity of precipitation events and their occurrence were not found to be directly impacted by the Edwards Plateau, however the location of the heaviest precipitation was shifted slightly northwest. Previous analysis of radar-retrieved precipitation [*Chen et al.*, 2015] suggested that the presence of the Balcones Escarpment might have affected certain types of precipitation (e.g., tropical/warm rain). Given the dense population in the metropolitan areas along the Balcones Escarpment, such a slight shift of precipitation or modification of certain precipitation type can significantly affect the location of dangerous flash flooding in the region. Unfortunately, prior

studies [e.g., *Chen et al.*, 2015; *Nielsen et al.*, 2016] did not convincingly identify the specific meteorological causes for the modification of precipitation by the Balcones Escarpment.

The Balcones Escarpment and the elevated terrain west of the escarpment (i.e., the Edwards Plateau) may exert influences on the atmosphere in two basic ways that can be described as thermal and dynamical effects (referred to as active and passive effects, respectively, by *De Wekker and Kossmann* [2015]).

Thermal effects of terrain can be induced simply by the elevation gradient or by unique land use categories or soil properties. When investigating wind fields in Texas during an intense heat wave, *Hu and Xue* [2016] found that a band of stronger winds developed during the afternoon along the terrain slope of Balcones Escarpment. They hypothesized that the wind maximum band was caused by the thermal contrast induced by the elevation gradient between the Edwards Plateau and the adjacent, low-lying plains east of the Balcones Escarpment. In addition to the elevation gradient, unique land properties (e.g., land use, soil type) may also lead to thermal effects of terrain [*Mahfouf et al.*, 1987; *McPherson et al.*, 2004]. The thermal effects of sloping terrain and their impact on precipitation and air pollution have been investigated for other mountains/plateaus [e.g., *Sun and Ogura*, 1979; *Sun and Wu*, 1992; *May and Wilczak*, 1993; *Koch et al.*, 2001; *Doran et al.*, 2002; *Rotach and Zardi*, 2007; *Zaitchik et al.*, 2007; *Pardyjak et al.*, 2009; *Sun and Zhang*, 2012; *Bao and Zhang*, 2013; *Hu et al.*, 2014; *Zhang et al.*, 2014; *Leo et al.*, 2015; *Li et al.*, 2015; *Miao et al.*, 2015; *Li et al.*, 2017]. Comparing to the thermal effects induced by elevation gradients, thermal effects of terrains induced by unique land properties have been less investigated.

As summarized previously [e.g., *Fernando et al.*, 2015; *Hu et al.*, 2016], the dynamic effects of mountainous terrain can cause different atmospheric processes, including barrier winds

[*Schwerdtfeger*, 1979; *Parish*, 1982; *Xu*, 1990; *McCauley and Sturman*, 1999; *Lee and Xue*, 2013; *Hu et al.*, 2016], flow around and over mountains [*Malkus*, 1955; *Smith*, 1982; *Pierrehumbert and Wyman*, 1985; *Chen and Feng*, 2001; *Hu and Liu*, 2005; *Yang and Chen*, 2008; *Jeglum et al.*, 2017; *Takane et al.*, 2017], wave motions [*Brown et al.*, 2003; *Smith*, 2004; *Grubisic et al.*, 2008; *Reinecke and Durran*, 2009; *Armi and Mayr*, 2011; *Jackson et al.*, 2013; *Serafin et al.*, 2017], wakes [*Epifanio and Rotunno*, 2005], gap winds [*Whiteman and Doran*, 1993; *Pan and Smith*, 1999; *Hitzl et al.*, 2014; *Wang et al.*, 2016], and flow separation [*Vosper et al.*, 2006; *Sheridan et al.*, 2007], to name a few examples. Dynamic effects generated by barriers to atmospheric flow have been shown to play important roles in development of precipitation [*Pedgley*, 1970; *Rotunno and Ferretti*, 2001; *Dettinger et al.*, 2004; *Houze and Medina*, 2005; *Medina et al.*, 2005; *Chen et al.*, 2013; *Lee and Xue*, 2013]. In *Wang et al.* [2016], several effects, including thermal upslope flows, lee-side convergence between around-mountain flows, and up-valley channeling flows, worked together in determining the preferred locations of convective initiation over the Dabie Mountains.

The detailed thermal and dynamic effects of the Edwards Plateau and Balcones Escarpment, however, have been rarely investigated except for few pilot studies, including *Hu and Xue* [2016] for a heat wave case and *Nielsen et al.* [2016] for three extreme precipitation cases. The meteorological consequences of the thermal and dynamic effects of the Balcones Escarpment, particularly precipitation development [*Nielsen et al.*, 2016], have not been clearly identified. One reason may be that the thermal and dynamic effects of the Balcones Escarpment were overwhelmed by the strong synoptic-scale forcing in the extreme precipitation cases investigated in Nielsen et al. (2016). To better understand the impact of the Edwards Plateau and Balcones Escarpment on precipitation in central Texas, we examine the climatological

precipitation patterns, timing, and location during August — a month when synoptically forced precipitation is less frequent — using nested regional model simulations and the Stage IV precipitation data. Even though extreme precipitation and flooding events in August may be less frequent than some other months (e.g., May) in the southern Great Plains, a better understanding of the effects of the Edwards Plateau and Balcones Escarpment in such a month with locally initiated precipitation dominating can help delineate their impacts on extreme precipitation and flooding events.

Warm-season convective precipitation in the U.S. Southern Great Plains (where Texas is located) is difficult to predict accurately, especially when using today's global climate models (GCMs) with coarse resolutions (e.g., 50-100 km grid spacing) [*Klein et al.*, 2006]. It is now commonly accepted that higher-resolution regional climate information can be obtained by dynamically downscaling coarse-resolution GCM outputs using mesoscale models [*Dickinson et al.*, 1989; *Giorgi*, 1990; *Jiao and Caya*, 2006]. Although some uncertainties exist in dynamical precipitation downscaling, higher-resolution downscaling simulations have been shown to be able to replicate the temporal and spatial distributions of convective weather for specific regions [*Gensini and Mote*, 2014].

In this study, the Weather Research and Forecasting (WRF) model [*Skamarock*, 2008] will be used to downscale August precipitation for 14 years (2002–2015) from a reanalysis dataset (which provides the lateral boundary conditions). WRF has been successfully used in a number of dynamical downscaling experiments at various horizontal resolutions [*Leung et al.*, 2006; *Lo et al.*, 2008; *Bukovsky and Karoly*, 2009; *Wang and Kotamarthi*, 2014]. For our study, we adopted the WRF configuration that has been documented to obtain the most accurate downscaled precipitation results over the Southern Great Plains. We describe this configuration,

other numerical model details, and the Stage IV precipitation data in section 2. Section 3 discusses the influence of the Edwards Plateau on August precipitation in Texas, as analyzed using the Stage IV data and simulation results. Section 4 summarizes and discusses the main findings.

2. Data and methods

2.1 Stage IV precipitation data and study period

The multi-sensor Stage IV precipitation data [*Lin*, 2011] are selected for this study because of their relatively long, consistent analysis record (archived continuously since January 2002), and their high temporal and spatial resolutions [*Herman and Schumacher*, 2016], which are essential to investigate the impact of topography's thermal effects (with a marked diurnal variation) on precipitation around central Texas. The Stage IV data are produced at the National Centers for Environmental Prediction (NCEP), and they combine the mosaiced hourly/6-hourly multi-sensor (including radar and gauges) precipitation analyses (called Stage III) produced by the twelve River Forecast Centers of the National Weather Service. Stage IV data cover the contiguous United States (CONUS) and have a grid spacing of about 4 km [*Petkovic and Kummerow*, 2012]. The data are available for hourly, 6-hourly, and daily intervals. Stage IV data display an overall agreement with surface observations, although the product has a tendency to underestimate both annual and seasonal means as compared to surface observations [*Nelson et al.*, 2016]. Stage IV precipitation data are available via http://data.eol.ucar.edu/codiac/dss/id=21.093.

Our study focuses on the regional climatology for a month when synoptically forced precipitation is at a minimum; otherwise, it may be difficult to identify the influence of the

Plateau for strongly forced synoptic events [*Nielsen et al.*, 2016]. Thus, we chose August as the study month and the past 14 years (2002-2015) as the study period to match the coverage of the Stage IV data (Fig. 1b). In August, thermal effects and their diurnal variation are most prominent [*Dai et al.*, 1999]. Also, in this month, the enhancement and westward extension of the Bermuda High make Texas less susceptible to the disturbance of the transient processes such as fronts and troughs, leading to less frequent episodes of synoptically forced precipitation near the Edwards Plateau [*Zhu and Liang*, 2013].

2.2 High-resolution dynamic downscaling of August climate

For this study, we investigate the August precipitation over Texas and the influence exerted by the Edwards Plateau and Balcones Escarpment. To this end, we downscaled August climate for 2002 to 2015 from the North American Regional Reanalysis (NARR) at 32-km horizontal resolution using the WRF model version 3.7.1 with a nested domain (Fig. 2) at a convection-allowing horizontal resolution (4 km), focusing on the southern Great Plains.

Accurate downscaling of summer precipitation remains a great challenge for most mesoscale models [*Liang et al.*, 2006; *Qiao and Liang*, 2015; *Gao et al.*, 2017], even at convection-allowing resolutions [*Sun et al.*, 2016]. Our previous dynamic downscaling of precipitation over the Great Plains for the past climate with the WRF model significantly underestimated warm-season precipitation over the Southern Great Plains and shifted the band of maximum precipitation to the Rockies and Nebraska [*Sun et al.*, 2016]; in most cases, the rain band was shifted northwestward, regardless of convection-allowing or convection-parameterizing configurations. Such a dry bias in the Great Plains was also previously reported [*Klein et al.*, 2006; *Lee et al.*, 2007; *Mearns et al.*, 2012; *Berg et al.*, 2013; *Tripathi and Dominguez*, 2013; *Harris and Lin*, 2014; *Ma et al.*, 2014]. Though not shown here, we

investigated possible reasons for the bias using a large set of sensitivity simulations with different physics parameterizations and both with and without spectral nudging [*Miguez-Macho et al.*, 2004]. We found that simply changing the physics parameterizations (e.g., cumulus, microphysics, land surface, boundary layer schemes) was unable to solve the bias problem in terms of the precipitation location. Applying spectral nudging, suggested by *Wang and Kotamarthi* [2014], led to more precipitation in the southern Great Plains and a best agreement with the Stage IV data. Successfully constraining the mesoscale simulation to follow the synoptic-scale driving fields by spectral nudging was key to reproducing the precipitation in the southern Great Plains in our case. This benefit, while maintaining the ability of the mesoscale models to develop small-scale dynamics, allowed successful applications of spectral nudging in dynamical downscaling of precipitation [*von Storch et al.*, 2000; *Mabuchi et al.*, 2002; *Miguez-Macho et al.*, 2004; *Lo et al.*, 2008; *Liu et al.*, 2012; *Spero et al.*, 2014; *Huang et al.*, 2016; *Paul et al.*, 2016; *García-Valdecasas Ojeda et al.*, 2017]. To achieve the best simulation of August precipitation climatology in this study, we used the spectral nudging configurations (including nudging strength, nudging height, and wave numbers) as suggested by *Wang and Kotamarthi* [2014] on the WRF downscaling simulations for the August of all 14 years. Particularly we adopted nudging wave numbers of 5 and 3 in the zonal and meridional directions over CONUS, thus relaxing long waves with wavelengths of ~1000 km to those of the driving fields.

Other WRF configurations for the August downscaling include the following: (1) two one-way nested domains (Fig. 2) are employed with horizontal grid resolutions of 20 for CONUS and 4 km for the south-central U.S.; (2) each domain has 44 vertical layers extending from the surface to 100 hPa; (3) all model domains use the Dudhia shortwave radiation [*Dudhia*, 1989], the rapid radiative transfer model (RRTM) [*Mlawer et al.*, 1997] for longwave radiation,

the Yonsei University (YSU) boundary layer scheme [*Hong et al.*, 2006; *Hu et al.*, 2013], and the Morrison microphysics scheme [*Morrison et al.*, 2009]; and (4) the Noah land surface scheme [*Chen and Dudhia*, 2001] coupled with a single-layer urban canopy model [*Kusaka et al.*, 2001]. Each continuous downscaling simulation starts at 0000UTC 1 August in each year of 2002-2015 and runs for the whole month. The model spins up for precipitation events in about 24 hours [*Lo et al.*, 2008; *Lucas-Picher et al.*, 2013; *Wang and Kotamarthi*, 2014].

2.3 WRF sensitivity simulations for 7 August 2011 to isolate/identify different effects

Since all the effects (including both thermal and dynamic effects) are simultaneously considered in a three-dimensional simulation, the specific effects of topography are normally hard to identify in one single simulation. Thus, modelers typically conduct a host of sensitivity simulations by changing one aspect of the configuration to isolate the cause of different effects. However, the expensive computational demand of the high-resolution dynamical downscaling over the selected domain for the past 14 Augusts (~170,000 service units were used) prohibits full-length sensitivity runs. Thus, to identify the specific effect of the Edwards Plateau, we conducted a large set of WRF simulations for a single day (7 August 2011) when the thermal and wind patterns near the Edwards Plateau are similar to those of the mean August patterns. For the chosen case of 7 August 2011, as documented previously in *Hu and Xue* [2016], sensitivity simulations use different soil properties, land uses, soil moisture, and terrain height to investigate how the escarpment and plateau affect the mesoscale circulations and boundary-layer development. Table 1 lists the configurations for the four most relevant sensitivity simulations. Note that on 7 August 2011, Texas was free of precipitation, allowing us to investigate the direct impact of the Edwards Plateau on vertical circulations while eliminating any conflating processes

or feedbacks of precipitation (e.g., latent heating associated with precipitation would lead to upward motion in the low troposphere, thus complicating the impact of the plateau).

3. Results

3.1 Daily mean precipitation amount in August 2002-2015 based on the Stage IV data

Based on our analysis of 14-year (i.e., 2002-2015) Stage IV precipitation data, the impact of the Edwards Plateau on the spatial distribution of precipitation is most prominent in August (Fig. 1b), probably due to strong radiative heating and fewer disturbances by strong synoptic scale transient processes (e.g., synoptic cold fronts). In this month, the total precipitation east of the Balcones Escarpment is suppressed as compared to that across the Edwards Plateau. Particularly at 1500 Central Standard Time (CST) (2100 UTC), the precipitation maximum over the Edwards Plateau appears distinct from the elongated precipitation minimum east of the escarpment (Fig. 3c,f). The precipitation gradient corresponds to the terrain of the Edwards Plateau (more precisely, the position of the Balcones Escarpment), suggesting that the Edwards Plateau and Balcones Escarpment play some roles in modifying the spatial distribution of precipitation in the region.

Mountains have been reported to affect precipitation in many places around the world through the mountains' thermal effect or orographic forcing effect [e.g., *Gao et al.*, 1981; *Tripoli and Cotton*, 1989b; *Wolyn and Mckee*, 1994; *Carbone and Tuttle*, 2008; *Liu et al.*, 2009; *He and Zhang*, 2010; *Sun and Zhang*, 2012; *Bao and Zhang*, 2013; *Zhang et al.*, 2014; *Wang et al.*, 2016]. On a clear summer afternoon, because of absorption of strong shortwave radiation, elevated terrain acts as a heat source, warming the near-surface air over the higher terrain as compared to adjacent, low-lying areas and producing a baroclinicity. As a result, a shallow (~4 km AGL) solenoid develops, comprised of an upslope wind along the sloping terrain and a

downward return flow over the adjacent, lower elevations. This thermally driven, local to regional scale circulation is commonly known as the Mountain-Plains Solenoid (MPS) circulation [*Tripoli and Cotton*, 1989a; *Wolyn and Mckee*, 1994; *Hu et al.*, 2014; *Hu and Xue*, 2016]. During the night, due to radiative cooling, the thermal gradient between mountains and the adjacent low-laying ground is reversed, as is the MPS circulation. The upward branch of the MPS circulation (over the mountains during the day and over the adjacent low-lying ground during the night) normally enhances precipitation [*He and Zhang*, 2010]. In most of the documented cases of precipitation modulation by the MPS circulation, the elevation difference (e.g., the Rockies, Tibetan Plateau, Loess Plateau) is greater than that between the Edwards Plateau and coastal plains. For the latter, the elevation difference is only 500-700 m (Fig. 1a). Thus, we need to carefully examine the possible causes of the precipitation maximum over the plateau.

3.2 Hourly mean precipitation frequency and amount

Since the thermal effect of any mountains has distinct diurnal variation [*He and Zhang*, 2010], simply focusing on the daily mean precipitation may obscure the different effects at different time of the day. Thus, we examined the frequency (Fig. 3) and rate (Fig. 4) of the hourly precipitation. Although the hourly precipitation rate is underestimated in the model simulations (as compared to the Stage IV data) at 0900 CST, the values and spatial patterns are realistic by 1500 CST (Fig. 4). Precipitation over the Edwards Plateau showed a prominent diurnal variation, with a dominant peak in the afternoon (1500-1800 CST) and a secondary peak in the early morning, 0700-0900 CST (Fig. 5).

The smaller, early morning peak in precipitation results from the eastward propagation of mesoscale convective systems (MCSs) initiated in the Rockies on the previous afternoon (Fig.

S1). The eastward propagation of MCSs provides the dominant nighttime precipitation in the central United States [*Dai et al.*, 1999; *Klein et al.*, 2006; *Qiao and Liang*, 2015]. Because the Edwards Plateau is near the southern and eastern extent of the nighttime propagation of these mesoscale features off of the Rockies, it receives the associated precipitation during the early morning (Fig. S1). The model successfully captures the timing of the eastward propagation of precipitation systems, but underestimates the precipitation intensity (Figs. 3d, 4c, and 5). It appears that the simulated precipitation maximum becomes weaker than observed during the eastward propagation process (Fig. 4a vs. 4c), leading to an early morning dry bias over Texas (Fig. 5), which is consistent with previously dynamic downscaling studies [*Klein et al.*, 2006; *Lee et al.*, 2007; *Berg et al.*, 2013; *Tripathi and Dominguez*, 2013; *Harris and Lin*, 2014; *Ma et al.*, 2014].

The dominant afternoon peak is presumably due to the locally initiated moist convection [*Liang et al.*, 2004]. Both the hourly frequency (Fig. 3b,c) and amount (Fig. 4b) of afternoon precipitation shows a coherent spatial pattern, with most precipitation events occurring in the eastern half of the Edwards Plateau and the precipitation east of the Balcones Escarpment suppressed, consistent with the spatial distribution of daily mean precipitation shown in Fig. 1b. The consistency between the daily mean precipitation and afternoon hourly precipitation indicates that the afternoon moist convection plays a dominant role in determining the spatial distribution of precipitation over this region of Texas in August. The dynamic downscaling results capture the spatial pattern of both afternoon precipitation frequency and amount. Although the simulations significantly overestimate precipitation frequency, the model accounts for all non-zero precipitation while very light precipitation may not be recorded in the Stage IV

data; this may partially explain the overestimation of frequency of afternoon precipitation in the model.

By examining the resemblance between hourly precipitation patterns and topography, the Edwards Plateau and Balcones Escarpment appear to play a great role in modulating afternoon precipitation, i.e., in enhancing the afternoon precipitation over the eastern Edwards Plateau and suppressing the afternoon precipitation east of the Balcones Escarpment. Since the WRF model successfully captures the general characteristics of the precipitation over Texas, confidence is gained for us to investigate the specific factors that modulate the precipitation patterns based on the modeling results. The afternoon precipitation gradient across the plateau, escarpment, and plains (Fig. 6b) corresponds well with the simulated upward motions (Fig. 6c). We first hypothesize that the upward branches of the MPS circulation enhances the afternoon precipitation, as reported in many previous studies [e.g., *He and Zhang*, 2010]. However, the spatial distribution of vertical velocity (Fig. 6c) contradicts such a hypothesis: the upward motion does not occur in the region with the largest slope (i.e., western side of the Edwards Plateau) as the MPS circulation would. Instead, upward motion occurs in some regions with a gentle slope, e.g., east of Dallas-Ft. Worth (DFW). Therefore, the MPS circulation associated with the sloping terrain does not provide a good explanation on the main upward motion found in the model.

Land surface processes are examined to search for the possible reasons for the specific pattern of the upward motions over the Edwards Plateau. It turns out that the spatial pattern of vertical velocity (Fig. 6c) matches that of sensible heat flux over the Edwards Plateau (Fig. 7c), which is further tied to the soil type (Fig. 7a). Dominant soil types 9 (clay loam) and 12 (clay), found underneath the upward motion over the Edwards Plateau, lead to relatively low latent heat fluxes and relatively high sensible heat fluxes while the dominant soil types 1 (sand) and 3

(sandy loam), found underneath the downward motion east of the Balcones Escarpment, lead to relatively high latent heat fluxes and relatively low sensible heat fluxes. Soil moisture alone cannot explain the spatial distribution of latent and sensible heat fluxes. Soil moisture over soil types 9 (clay loam) and 12 (clay) is actually higher than soil types 1 (sand) and 3 (sandy loam) east of the Balcones Escarpment (Fig. 7d); however, the latent heat fluxes over clay-based soil types (9 and 12) are lower and sensible heat fluxes are higher.

To examine these relationships in more detail, we reviewed the hydraulic properties of different soil types used by the WRF model. The marked differences between clay-based soil types 9 and 12 and sand-based soil types 1 and 3 are with the dry-soil moisture threshold (DRYSMC) and wilting-point soil moisture (WLTSMC) of the soil. For any given soil type, the Noah land-surface model uses the same value for these two parameters (Table 2). These parameters play an important role in dictating evapotranspiration by scaling potential evapotranspiration through a moisture availability parameter β [*Betts et al.*, 1997; *Chen and Dudhia*, 2001]:

$$\beta = \frac{\Theta - \Theta_w}{\Theta_{ref} - \Theta_w} \qquad (1)$$

where Θ is volumetric soil moisture content, Θ_{ref} is the field capacity, and Θ_w is either the soil moisture at the wilting point (WLTSMC) for vegetation canopy evapotranspiration or the dry-soil moisture threshold (DRYSMC) for ground surface direct evaporation. When the soil moisture becomes lower than DRYSMC or WLTSMC, β is set as zero and surface evapotranspiration is shut off. The clay-based soil types have higher values of DRYSMC and WLTSMC than sand-based types (Fig. 7e), by a factor of as high as 14 (Table 2). Because DRYSMC and WLTSMC values can be high (as high as 0.138 $m^3\ m^{-3}$) for clay-based soil types (which dominate over the eastern Edwards Plateau), the actual soil moisture values are more

likely to decrease below the DRYSMC and WLTSMC of clay-based as opposed to sand-based soils, leading to nearly zero β (Fig. 7f) for the former soil types. Thus, one would expect lower latent heat fluxes (Fig. 7b) and consequently high sensible heat fluxes in regions with clay soils (Fig. 7c).

The simulated different behavior of surface fluxes over clay and sand is consistent with soil granulometry. Sand is composed of relatively coarse particles with diameter between 2 mm and 50 μm while clay is composed of fine particles with diameter less than 2 μm [*Liu et al.*, 2013]. Sandy soil is coarse textured, allowing water to easily circulate via capillary motion to reach the surface or plant roots where it can be evaporated or absorbed (and eventually released from leaves) [*Mahfouf et al.*, 1987; *Fast and Mccorcle*, 1990]. In contrast, in fine textured clay soil, the capillary motion is quite slow and it is hard for water to circulate and participate in evapotranspiration, thus leading to suppressed latent fluxes (consequently enhanced sensible heat fluxes) during the day [*Mahfouf et al.*, 1987; *Fast and Mccorcle*, 1991]. The high sensible heat fluxes over clay-based soils (Fig. 7c) will induce upward motion (Fig. 6c) that helps to trigger the afternoon moist convection under favorable conditions (Fig. 6b).

The west-to-east vertical cross-sections of vertical velocity and rain water through DFW further corroborate the above analysis (Fig. 8). Upward motion occurs almost exactly over the clay-based soil types (shaded in dark red-brown) while downward motion occurs over the sand-based soil types (shaded in bright yellow), with a solenoidal circulation being the strongest along the clay-sand boundaries (Fig. 8a). Latent heat flux is more (less) likely to shut down over the clay- (sand-) based soil due to its high (low) values of DRYSMC and WLTSMC, consequently leading to high (low) sensible heat flux and upward (downward) motion. The resulting downward motion over the sandy soils suppresses the precipitation east of DFW while the

upward motion over the clay soils triggers more precipitation west of the Balcones Escarpment (Fig. 8b). The impact of different surface energy balance (or partition between sensible and latent heat fluxes) on precipitation shown in this study is also corroborated by large eddy simulations conducted by *Kang* [2016], in which a higher Bowen ratio (i.e., more sensible heat flux relative to latent flux) is shown to more likely trigger afternoon moist convection. This study is also consistent with previous observational studies [e.g., *Taylor et al.*, 2012] that show more afternoon rainfall over areas with enhanced sensible heat flux.

Due to the companion presence of upward and downward motions, local circulations (named as soil-type circulation) are developed over some regions, e.g., east of DFW. A similar local circulation due to a comparable spatial pattern of vertical velocities along the Balcones Escarpment was previously reported in a case study on 7 August 2011 where the local circulations were, however, attributed to the MPS circulation as a result of the terrain height difference [*Hu and Xue*, 2016]. Yet, the gentle terrain slope east of DFW (Fig. 8) disproves the MPS circulation hypothesis but corroborates the soil-type circulation idea.

3.3 Isolate and identify different effects using WRF sensitivity simulations for 7 August 2011

To further isolate and identify the thermal and dynamic effects of the Edwards Plateau and Balcones Escarpment, sensitivity simulations are considered. Given that the mean surface and boundary-layer patterns associated with the Edwards Plateau in August is similar to that on 7 August 2011 as reported by *Hu and Xue* [2016], we conducted a large set of sensitivity simulations using WRF with different configurations (with the four most relevant ones listed in Table 1) for the clear case of 7 August 2011. Figure 9 displays the simulation results in the afternoon of this day.

After changing the soil types 1 (sand), 9 (clay loam), and 12 (clay) to 3 (sandy loam) in simulation 2 to homogenize the soil types in the region of interest (Fig. 9h), the large values of sensible heat flux over the original clay-based soil types (12 and 9) are significantly reduced (Fig. 9k), as is the associated upward motion except for that over the southern tip of the Edwards Plateau (Fig. 9l). The band of maximum wind along the Balcones Escarpment (Fig. 9f), due to the superimposed local circulation and prevailing southerly/southeasterly winds explained by *Hu and Xue* [2016], is virtually gone when the main soil-type contrast is removed in simulation 2 (Fig. 9m). Thus, simulation 2 confirms that the upward motion and local circulations are mostly dictated by the soil-type heterogeneity rather than the terrain height gradients as previously thought.

To further identify the most important hydraulic properties of the different soil types, simulation 3 swaps the values for DRYSMC and WLTSMC (Table 1) between clay-based soils (9 and 12) and sand (1), with soil types and all other configuration variables remaining the same. In this simulation, with spuriously high DRYSMC and WLTSMC assigned for sand, soil moisture values for sand now reach the dry-soil moisture threshold and wilting-point soil moisture thresholds (Fig. 9u), thus leading to nearly zero latent heat flux (Fig. 9q) and consequently high sensible heat flux (Fig. 9r) and upward motion (Fig. 9s). Thus, the local circulation pattern east of DFW is now reversed. Superimposing the surface branch of this reversed local circulation on the prevailing southerly/southeasterly winds leads to a wind-minimum band near the surface east of DFW (Fig. 9t), in contrast to the wind-maximum band in the control simulation (Fig. 9f). Thus, simulation 3 successfully identifies critical parameters DRYSMC and WLTSMC as being the most important in determining the relative strength of the surface heat fluxes and the vertical velocities and local circulations associated with them.

Simulation 4 is identical to simulation 1 (control) except that the terrain of the Edwards Plateau is removed (Fig. 9w). In this simulation, the spatial patterns of vertical velocity (Fig. 9z) and surface wind maximum along the Balcones Escarpment (Fig. 9aa) are similar to those of control simulation, again indicating that the terrain plays a secondary role in dictating the vertical motions and local circulations. The weakened upward motion over the southern tip of the Edwards Plateau (as compared to the control simulation) indicates that the terrain of Edwards Plateau mostly enhances upward motion in the afternoon over the southern end of the Plateau.

Some other sensitivity simulations were also conducted, e.g., changing soil moisture, changing land use categories. All of them further confirm that soil type plays the most important role in dictating the surface fluxes (and subsequently vertical velocities and local circulations) while other factors play secondary or negligible roles in this case. Thus, the sensitivity simulations for this case study confirm and further prove the conclusions derived from the 14-year August simulations that clay-based soils enhance the upward motion in the afternoon over the Edwards Plateau and Balcones Escarpment.

4. Conclusions and discussion

The Balcones Escarpment in central Texas is a sloping terrain region between the Edwards Plateau and the coastal plain. The metropolitan areas located along the Balcones Escarpment are prone to heavy precipitation and flooding events. The meteorological impacts of the Edwards Plateau and Balcones Escarpment have not been well understood. The indeterminate impacts are investigated in this study using the Stage IV precipitation data, convection-allowing dynamic downscaling with spectral nudging, and sensitivity simulations for a representative case.

Based on our analysis of 14-year (i.e., 2002-2015) Stage IV precipitation data, the role of the Edwards Plateau in modulating precipitation distribution is most prominent in August. In this month, the total precipitation east of the Balcones Escarpment is suppressed. The precipitation over the eastern part of the Edwards Plateau appears separated from the other precipitation area in the east, south, and west. Locally initiated moist convection in the afternoon contributes most to the total precipitation during this month in the region. The dynamically downscaled simulations nicely capture the spatial patterns of both afternoon precipitation frequency and amount, matching the simulated upward motions. The upward motion does not occur in the region with the largest slope (i.e., western side of the Edwards Plateau); instead, it occurs in some regions with a gentle slope, e.g., east of DFW. Thus, the Mountain-Plains Solenoid (MPS) circulation (which is supposed to be most prominent at places with the largest horizontal elevation differences) cannot explain the dominant vertical motions.

Land surface processes are examined to search for possible explanation for the specific pattern of upward motions over the Edwards Plateau. In fact, the spatial pattern of vertical velocity matches that of surface sensible heat fluxes quite well, which is found to be primarily tied to the soil type. The clay-based soil types dominant over the Edwards Plateau have a relatively higher dry-soil moisture threshold and wilting-point soil moisture than their sandy counterparts dominant over the plain to the east. Thus, clay-based soils can retain more of their soil moisture, reducing evapotranspiration and limiting latent heat fluxes, consequently leading to higher sensible heat fluxes. As a result of high sensible heat flux, vertical motion is induced, helping to trigger afternoon moist convection over the Edwards Plateau under favorable conditions. Sensitivity simulations for a representative day confirm and further prove this conclusion.

The impact of soil hydraulic parameters on precipitation has been investigated previously, mostly in Hungary [*Horvath et al.*, 2009; *Acs et al.*, 2010; *Acs et al.*, 2015] and in China [*He et al.*, 2016]. Most of these previous investigations demonstrated certain sensitivities of precipitation to some soil hydraulic parameters; in particular, *He et al.* [2016] reported a large sensitivity of WRF-simulated precipitation to wilting point soil moisture contents. However, none of the previous studies revealed a clear cause-and-effect relationship between soil hydraulic parameters and precipitation. Our study clearly shows that the high dry-soil moisture threshold and wilting-point soil moisture trigger more afternoon moist convection over the Edwards Plateau and Balcones Escarpment in August. This study only represents an initial investigation of effects of the Edward Plateau and Balcones Escarpment on precipitation. Further investigation for other episodes/months with more extreme rainfall and flooding events is warranted.

In addition, we obtained a better understanding of the band of afternoon, near-surface wind maxima along the Balcones Escarpment, previously attributed to superimposing the MPS circulation onto the prevailing southerly/southeasterly winds [*Hu and Xue*, 2016]. These wind maxima are still due to the local circulation pattern, but this pattern is now recognized to have not resulted from the thermal contrast induced by the terrain height differences but rather from the thermal contrast between different soil types. Other types of local circulations, e.g., MPS circulation, land-sea breeze circulation, vegetation breeze circulation, have been reported extensively [e.g., *Ookouchi et al.*, 1984; *Mahfouf et al.*, 1987; *Yan and Anthes*, 1988; *Avissar and Pielke*, 1989; *Schadler*, 1990; *Fast and Mccorcle*, 1991; *Segal and Arritt*, 1992; *Lynn et al.*, 1998; *Miller et al.*, 2003; *McPherson et al.*, 2004; *McPherson and Stensrud*, 2005; *McPherson*, 2007; *Porson et al.*, 2007; *Crosman and Horel*, 2010; *He and Zhang*, 2010; *Steele et al.*, 2013; 2015; *Massey et al.*, 2017]. This is the first time the soil-type circulation is clearly demonstrated

in three-dimensional simulations to our best knowledge. The circulation can also be called soil-type breeze.

In addition to modulating precipitation distribution, the soil-type circulation may also have important implications for air quality during clear days with significant solar forcing. The downward branch of the circulation suppresses boundary-layer development east of the Balcones Escarpment, which may enhance air pollution in the region in a similar way as the downward branch of MPS circulations [*De Wekker*, 2008; *Steyn et al.*, 2013; *Hu et al.*, 2014; *De Wekker and Kossmann*, 2015; *Rendon et al.*, 2015].

Acknowledgement. The project described in this publication was supported by Grant G15AP00131 from the United States Geological Survey. Its contents are solely the responsibility of the authors and do not necessarily represent the views of the South Central Climate Science Center or the USGS. This manuscript is submitted for publication with the understanding that the United States Government is authorized to reproduce and distribute reprints for Governmental purposes. The second author was supported by NSF grants AGS-0941491, AGS-1046171, AGS-1046081, and AGS-1261776. Discussion with Dr. Yuning Shi is helpful. Computations were performed at the Texas Advanced Computing Center (TACC) and San Diego Supercomputer Center (SDSC). The NARR data set was downloaded from https://rda.ucar.edu/datasets/ds608.0/, and the Stage IV precipitation data were downloaded from http://data.eol.ucar.edu/codiac/dss/id=21.093. Model data produced from this study have been archived at Center for Analysis and Prediction of Storms, University of Oklahoma, and are available from the authors upon request.

512

References

Acs, F., A. Horvath, H. Breuer, and F. Rubel (2010), Effect of soil hydraulic parameters on the local convective precipitation, *Meteorol Z*, *19*(2), 143-153, doi:10.1127/0941-2948/2010/0435.

Acs, F., K. Rajkai, H. Breuer, T. Mona, and A. Horvath (2015), Soil-atmosphere relationships: The Hungarian perspective, *Open Geosci*, *7*(1), 395-406, doi:10.1515/geo-2015-0036.

Armi, L., and G. J. Mayr (2011), The Descending Stratified Flow and Internal Hydraulic Jump in the Lee of the Sierras, *J Appl Meteorol Clim*, *50*(10), 1995-2011, doi:Doi 10.1175/Jamc-D-10-05005.1.

Ashley, S. T., and W. S. Ashley (2008), Flood fatalities in the United States, *J Appl Meteorol Clim*, *47*(3), 805-818, doi:10.1175/2007jamc1611.1.

Avissar, R., and R. A. Pielke (1989), A Parameterization of Heterogeneous Land Surfaces for Atmospheric Numerical-Models and Its Impact on Regional Meteorology, *Monthly Weather Review*, *117*(10), 2113-2136, doi:Doi 10.1175/1520-0493(1989)117<2113:Apohls>2.0.Co;2.

Bao, X. H., and F. Q. Zhang (2013), Impacts of the mountain-plains solenoid and cold pool dynamics on the diurnal variation of warm-season precipitation over northern China, *Atmos Chem Phys*, *13*(14), 6965-6982, doi:10.5194/acp-13-6965-2013.

Berg, A., K. Findell, B. R. Lintner, P. Gentine, and C. Kerr (2013), Precipitation Sensitivity to Surface Heat Fluxes over North America in Reanalysis and Model Data, *J Hydrometeorol*, *14*(3), 722-743, doi:10.1175/Jhm-D-12-0111.1.

Betts, A. K., F. Chen, K. E. Mitchell, and Z. I. Janjic (1997), Assessment of the land surface and boundary layer models in two operational versions of the NCEP Eta Model using FIFE data, *Monthly Weather Review*, *125*(11), 2896-2916, doi:Doi 10.1175/1520-0493(1997)125<2896:Aotlsa>2.0.Co;2.

Brown, A. R., M. Athanassiadou, and N. Wood (2003), Topographically induced waves within the stable boundary layer, *Q J Roy Meteor Soc*, *129*(595), 3357-3370, doi:10.1256/qj.02.176.

Bukovsky, M. S., and D. J. Karoly (2009), Precipitation Simulations Using WRF as a Nested Regional Climate Model, *J Appl Meteorol Clim*, *48*(10), 2152-2159, doi:10.1175/2009jamc2186.1.

Carbone, R. E., and J. D. Tuttle (2008), Rainfall occurrence in the US warm season: The diurnal cycle, *J Climate*, *21*(16), 4132-4146, doi:10.1175/2008jcli2275.1.

Chen, C. Y., Y. L. Chen, C. S. Chen, P. L. Lin, and C. L. Liu (2013), Revisiting the Heavy Rainfall Event over Northern Taiwan on 3 June 1984, *Terr Atmos Ocean Sci*, *24*(6), 999-1020, doi:Doi 10.3319/Tao.2013.07.04.01(a).

Chen, F., and J. Dudhia (2001), Coupling an advanced land surface-hydrology model with the Penn State-NCAR MM5 modeling system. Part I: Model implementation and sensitivity,

Monthly Weather Review, *129*(4), 569-585, doi:Doi 10.1175/1520-0493(2001)129<0569:Caalsh>2.0.Co;2.

Chen, S., J. Zhang, E. Mullens, Y. Hong, A. Behrangi, Y. D. Tian, X. M. Hu, J. J. Hu, Z. X. Zhang, and X. H. Zhang (2015), Mapping the Precipitation Type Distribution Over the Contiguous United States Using NOAA/NSSL National Multi-Sensor Mosaic QPE, *Ieee T Geosci Remote*, *53*(8), 4434-4443, doi:10.1109/Tgrs.2015.2399015.

Chen, Y. L., and J. H. Feng (2001), Numerical simulations of airflow and cloud distributions over the windward side of the island of Hawaii. Part I: The effects of trade wind inversion, *Monthly Weather Review*, *129*(5), 1117-1134, doi:Doi 10.1175/1520-0493(2001)129<1117:Nsoaac>2.0.Co;2.

Crosman, E. T., and J. D. Horel (2010), Sea and Lake Breezes: A Review of Numerical Studies, *Boundary-Layer Meteorology*, *137*(1), 1-29, doi:DOI 10.1007/s10546-010-9517-9.

Dai, A., F. Giorgi, and K. E. Trenberth (1999), Observed and model-simulated diurnal cycles of precipitation over the contiguous United States, *J Geophys Res-Atmos*, *104*(D6), 6377-6402, doi:Doi 10.1029/98jd02720.

De Wekker, S. F. J. (2008), Observational and numerical evidence of depressed convective boundary layer heights near a mountain base, *J Appl Meteorol Clim*, *47*(4), 1017-1026, doi:10.1175/2007jamc1651.1.

De Wekker, S. F. J., and M. Kossmann (2015), Convective boundary layer heights over mountainous terrain – A review of concepts –, *Frontiers in Earth Science*, *3*, doi:10.3389/feart.2015.00077.

Dettinger, M., K. Redmond, and D. Cayan (2004), Winter orographic precipitation ratios in the Sierra Nevada - Large-scale atmospheric circulations and hydrologic consequences, *J Hydrometeorol*, *5*(6), 1102-1116, doi:Doi 10.1175/Jhm-390.1.

Dickinson, R. E., R. M. Errico, F. Giorgi, and G. T. Bates (1989), A Regional Climate Model for the Western United-States, *Climatic Change*, *15*(3), 383-422.

Doran, J. C., J. D. Fast, and J. Horel (2002), The VTMX 2000 campaign, *B Am Meteorol Soc*, *83*(4), 537-551, doi:Doi 10.1175/1520-0477(2002)083<0537:Tvc>2.3.Co;2.

Dudhia, J. (1989), Numerical Study of Convection Observed during the Winter Monsoon Experiment Using a Mesoscale Two-Dimensional Model, *J Atmos Sci*, *46*(20), 3077-3107, doi:Doi 10.1175/1520-0469(1989)046<3077:Nsocod>2.0.Co;2.

Epifanio, C. C., and R. Rotunno (2005), The dynamics of orographic wake formation in flows with upstream blocking, *J Atmos Sci*, *62*(9), 3127-3150, doi:Doi 10.1175/Jas3523.1.

Fast, J. D., and M. D. Mccorcle (1990), A 2-Dimensional Numerical Sensitivity Study of the Great-Plains Low-Level Jet, *Monthly Weather Review*, *118*(1), 151-163, doi:Doi 10.1175/1520-0493(1990)118<0151:Atdnss>2.0.Co;2.

Fast, J. D., and M. D. Mccorcle (1991), The Effect of Heterogeneous Soil-Moisture on a Summer Baroclinic Circulation in the Central United-States, *Monthly Weather Review*, *119*(9), 2140-2167, doi:Doi 10.1175/1520-0493(1991)119<2140:Teohsm>2.0.Co;2.

Fernando, H. J. S., et al. (2015), THE MATERHORN Unraveling the Intricacies of Mountain Weather, *B Am Meteorol Soc*, *96*(11), doi:10.1175/Bams-D-13-00131.1.

Gao, Y., L. R. Leung, C. Zhao, and S. Hagos (2017), Sensitivity of US summer precipitation to model resolution and convective parameterizations across gray zone resolutions, *J Geophys Res-Atmos*, *122*(5), 2714-2733, doi:10.1002/2016jd025896.

Gao, Y. X., M. C. Tang, S. W. Luo, Z. B. Shen, and C. Li (1981), Some Aspects of Recent Research on the Qinghai-Xizang Plateau Meteorology, *B Am Meteorol Soc*, *62*(1), 31-35, doi:Doi 10.1175/1520-0477(1981)062<0031:Saorro>2.0.Co;2.

García-Valdecasas Ojeda, M., S. R. Gámiz-Fortis, Y. Castro-Díez, and M. J. Esteban-Parra (2017), Evaluation of WRF capability to detect dry and wet periods in Spain using drought indices, *Journal of Geophysical Research: Atmospheres*, *122*(3), 1569-1594, doi:10.1002/2016JD025683.

Gensini, V. A., and T. L. Mote (2014), Estimations of Hazardous Convective Weather in the United States Using Dynamical Downscaling, *J Climate*, *27*(17), 6581-6589, doi:10.1175/Jcli-D-13-00777.1.

Giorgi, F. (1990), Simulation of Regional Climate Using a Limited Area Model Nested in a General-Circulation Model, *J Climate*, *3*(9), 941-963, doi:Doi 10.1175/1520-0442(1990)003<0941:Sorcua>2.0.Co;2.

Gleason, K. L., J. H. Lawrimore, D. H. Levinson, T. R. Karl, and D. J. Karoly (2008), A revised US Climate Extremes Index, *J Climate*, *21*(10), 2124-2137, doi:10.1175/2007jcli1883.1.

Groisman, P. Y., and R. W. Knight (2008), Prolonged dry episodes over the conterminous united states: New tendencies emerging during the last 40 years, *J Climate*, *21*(9), 1850-1862, doi:10.1175/2007jcli2013.1.

Grubisic, V., et al. (2008), THE TERRAIN-INDUCED ROTOR EXPERIMENT A Field Campaign Overview Including Observational Highlights, *B Am Meteorol Soc*, *89*(10), 1513-1533, doi:Doi 10.1175/2008bams2487.1.

Harris, L. M., and S. J. Lin (2014), Global-to-Regional Nested Grid Climate Simulations in the GFDL High Resolution Atmospheric Model, *J Climate*, *27*(13), 4890-4910, doi:10.1175/Jcli-D-13-00596.1.

He, H. Z., and F. Q. Zhang (2010), Diurnal Variations of Warm-Season Precipitation over Northern China, *Monthly Weather Review*, *138*(4), 1017-1025, doi:10.1175/2010mwr3356.1.

He, J. J., Y. Yu, L. J. Yu, C. M. Yin, N. Liu, S. P. Zhao, and X. Chen (2016), Effect of soil texture and hydraulic parameters on WRF simulations in summer in east China, *Atmospheric Science Letters*, *17*(10), 538-547, doi:10.1002/asl.690.

Herman, G. R., and R. S. Schumacher (2016), Extreme Precipitation in Models: An Evaluation, *Weather Forecast*, *31*(6), 1853-1879, doi:10.1175/waf-d-16-0093.1.

Hitzl, D. E., Y. L. Chen, and H. V. Nguyen (2014), Numerical Simulations and Observations of Airflow through the 'Alenuihaha Channel, Hawaii, *Monthly Weather Review*, *142*(12), 4696-4718, doi:Doi 10.1175/Mwr-D-13-00312.1.

Hong, S. Y., Y. Noh, and J. Dudhia (2006), A new vertical diffusion package with an explicit treatment of entrainment processes, *Mon Weather Rev*, *134*(9), 2318-2341, doi:Doi 10.1175/Mwr3199.1.

Horvath, A., F. Acs, and H. Breuer (2009), On the relationship between soil, vegetation and severe convective storms: Hungarian case studies, *Atmos Res*, *93*(1-3), 66-81, doi:10.1016/j.atmosres.2008.10.007.

Houze, R. A., and S. Medina (2005), Turbulence as a mechanism for orographic precipitation enhancement, *J Atmos Sci*, *62*(10), 3599-3623, doi:Doi 10.1175/Jas3555.1.

Hu, X.-M., P. M. Klein, and M. Xue (2013), Evaluation of the updated YSU planetary boundary layer scheme within WRF for wind resource and air quality assessments, *J Geophys Res-Atmos*, *118*(18), 10490-10505, doi:10.1002/jgrd.50823.

Hu, X.-M., X. Li, M. Xue, D. Wu, and J. D. Fuentes (2016), The Formation of Barrier Winds East of the Loess Plateau and Their Effects on Dispersion Conditions in the North China Plains, *Boundary-Layer Meteorology*, *161*(1), 145-163, doi:10.1007/s10546-016-0159-4.

Hu, X.-M., Z. Q. Ma, W. L. Lin, H. L. Zhang, J. L. Hu, Y. Wang, X. B. Xu, J. D. Fuentes, and M. Xue (2014), Impact of the Loess Plateau on the atmospheric boundary layer structure and air quality in the North China Plain: A case study, *Sci Total Environ*, *499*, 228-237, doi:DOI 10.1016/j.scitotenv.2014.08.053.

Hu, X.-M., and M. Xue (2016), Influence of Synoptic Sea-Breeze Fronts on the Urban Heat Island Intensity in Dallas–Fort Worth, Texas, *Monthly Weather Review*, *144*(4), 1487-1507, doi:10.1175/mwr-d-15-0201.1.

Hu, X. M., and S. Liu (2005), Numerical Simulation of Land Surface Process and Atmosphere Boundary Layer Structure over Small Hill Underlying Surface, *Journal of Applied Meterological Science*, *16*(1), 13-23.

Huang, W.-R., Y.-H. Chang, H.-H. Hsu, C.-T. Cheng, and C.-Y. Tu (2016), Dynamical downscaling simulation and future projection of summer rainfall in Taiwan: Contributions from different types of rain events, *Journal of Geophysical Research: Atmospheres*, n/a-n/a, doi:10.1002/2016JD025643.

Jackson, P. L., G. Mayr, and S. Vosper (2013), Dynamically-Driven Winds, in *Mountain Weather Research and Forecasting: Recent Progress and Current Challenges*, edited by F. K. Chow, S. F. J. De Wekker and B. J. Snyder, pp. 121-218, Springer Netherlands, Dordrecht, doi:10.1007/978-94-007-4098-3_3.

Jeglum, M. E., S. W. Hoch, D. D. Jensen, R. Dimitrova, and Z. Silver (2017), Large Temperature Fluctuations due to Cold-Air Pool Displacement along the Lee Slope of a Desert Mountain, *J Appl Meteorol Clim*, *56*(4), 1083-1098, doi:10.1175/jamc-d-16-0202.1.

Jiao, Y. J., and D. Caya (2006), An investigation of summer precipitation simulated by the Canadian Regional Climate Model, *Monthly Weather Review*, *134*(3), 919-932, doi:Doi 10.1175/Mwr3103.1.

Kang, S.-L. (2016), Regional Bowen ratio controls on afternoon moist convection: A large eddy simulation study, *Journal of Geophysical Research: Atmospheres*, n/a-n/a, doi:10.1002/2016JD025567.

Klein, S. A., X. N. Jiang, J. Boyle, S. Malyshev, and S. C. Xie (2006), Diagnosis of the summertime warm and dry bias over the U.S. Southern Great Plains in the GFDL climate model using a weather forecasting approach, *Geophys Res Lett*, *33*(18), doi:L18805, 10.1029/2006gl027567.

Koch, S. E., F. Q. Zhang, M. L. Kaplan, Y. L. Lin, R. Weglarz, and C. M. Trexler (2001), Numerical simulations of a gravity wave event over CCOPE. Part III: The role of a mountain-plains solenoid in the generation of the second wave episode, *Monthly Weather Review*, *129*(5), 909-933, doi:Doi 10.1175/1520-0493(2001)129<0909:Nsoagw>2.0.Co;2.

Kusaka, H., H. Kondo, Y. Kikegawa, and F. Kimura (2001), A simple single-layer urban canopy model for atmospheric models: Comparison with multi-layer and slab models, *Boundary-Layer Meteorology*, *101*(3), 329-358, doi:Doi 10.1023/A:1019207923078.

Lee, J. G., and M. Xue (2013), A study on a snowband associated with a coastal front and cold-air damming event of 3-4 February 1998 along the eastern coast of the Korean Peninsula, *Adv Atmos Sci*, *30*(2), 263-279, doi:DOI 10.1007/s00376-012-2088-6.

Lee, M. I., et al. (2007), Sensitivity to horizontal resolution in the AGCM simulations of warm season diurnal cycle of precipitation over the United States and northern Mexico, *J Climate*, *20*(9), 1862-1881, doi:10.1175/Jcl14090.1.

Leo, L. S., H. J. S. Fernando, and S. Di Sabatino (2015), Near-surface flow in complex terrain with coastal and urban influence, *Environ Fluid Mech*, *15*(2), 349-372, doi:10.1007/s10652-013-9327-y.

Leung, L. R., Y. H. Kuo, and J. Tribbia (2006), Research needs and directions of regional climate modeling using WRF and CCSM, *B Am Meteorol Soc*, *87*(12), 1747-1751, doi:10.1175/Bams-887-12-1747.

Li, J., T. Chen, and N. Li (2017), Diurnal variation of summer precipitation across the central Tianshan Mountain, *J Appl Meteorol Clim*, *0*(0), null, doi:10.1175/jamc-d-16-0265.1.

Li, X., X. Xia, L. Wang, R. Cai, L. Zhao, Z. Feng, Q. Ren, and K. Zhao (2015), The role of foehn in the formation of heavy air pollution events in Urumqi, China, *J Geophys Res-Atmos*, *120*(11), 5371-5384, doi:10.1002/2014jd022778.

Liang, X. Z., L. Li, A. Dai, and K. E. Kunkel (2004), Regional climate model simulation of summer precipitation diurnal cycle over the United States, *Geophys Res Lett*, *31*(24), doi:L24208, 10.1029/2004gl021054.

Liang, X. Z., J. P. Pan, J. H. Zhu, K. E. Kunkel, J. X. L. Wang, and A. Dai (2006), Regional climate model downscaling of the U.S. summer climate and future change, *J Geophys Res-Atmos*, *111*(D10), doi:D10108, 10.1029/2005jd006685.

Lin, Y. (2011), GCIP/EOP Surface: Precipitation NCEP/EMC 4KM Gridded Data (GRIB) Stage IV Data, edited by U. N.-E. O. Laboratory, UCAR/NCAR - Earth Observing Laboratory, doi:http://data.eol.ucar.edu/dataset/21.093.

Liu, P., A. P. Tsimpidi, Y. Hu, B. Stone, A. G. Russell, and A. Nenes (2012), Differences between downscaling with spectral and grid nudging using WRF, *Atmos Chem Phys*, *12*(8), 3601-3610, doi:10.5194/acp-12-3601-2012.

Liu, S., Y. Wei, W. M. Post, R. B. Cook, K. Schaefer, and M. M. Thornton (2013), The Unified North American Soil Map and its implication on the soil organic carbon stock in North America, *Biogeosciences*, *10*(5), 2915-2930, doi:10.5194/bg-10-2915-2013.

Liu, X. D., A. J. Bai, and C. H. Liu (2009), Diurnal variations of summertime precipitation over the Tibetan Plateau in relation to orographically-induced regional circulations, *Environ Res Lett*, *4*(4), doi:045203, 10.1088/1748-9326/4/4/045203.

Lo, J. C. F., Z. L. Yang, and R. A. Pielke (2008), Assessment of three dynamical climate downscaling methods using the Weather Research and Forecasting (WRF) model, *J Geophys Res-Atmos*, *113*(D9), doi:D09112, 10.1029/2007jd009216.

Lucas-Picher, P., F. Boberg, J. H. Christensen, and P. Berg (2013), Dynamical Downscaling with Reinitializations: A Method to Generate Finescale Climate Datasets Suitable for Impact Studies, *J Hydrometeorol*, *14*(4), 1159-1174, doi:10.1175/Jhm-D-12-063.1.

Lynn, B. H., W. K. Tao, and P. J. Wetzel (1998), A study of landscape-generated deep moist convection, *Monthly Weather Review*, *126*(4), 928-942, doi:Doi 10.1175/1520-0493(1998)126<0928:Asolgd>2.0.Co;2.

Ma, H. Y., et al. (2014), On the Correspondence between Mean Forecast Errors and Climate Errors in CMIP5 Models, *J Climate*, *27*(4), 1781-1798, doi:10.1175/Jcli-D-13-00474.1.

Mabuchi, K., Y. Sato, and H. Kida (2002), Verification of the climatic features of a regional climate model with BAIM, *J Meteorol Soc Jpn*, *80*(4), 621-644, doi:DOI 10.2151/jmsj.80.621.

Mahfouf, J. F., E. Richard, and P. Mascart (1987), The Influence of Soil and Vegetation on the Development of Mesoscale Circulations, *J Clim Appl Meteorol*, *26*(11), 1483-1495, doi:Doi 10.1175/1520-0450(1987)026<1483:Tiosav>2.0.Co;2.

Malkus, J. S. (1955), The Effects of a Large Island Upon the Trade-Wind Air Stream, *Q J Roy Meteor Soc*, *81*(350), 538-550, doi:DOI 10.1002/qj.49708135003.

Massey, J. D., W. J. Steenburgh, S. W. Hoch, and D. D. Jensen (2017), Simulated and Observed Surface Energy Fluxes and Resulting Playa Breezes during the MATERHORN Field Campaigns, *J Appl Meteorol Clim*, *56*(4), 915-935, doi:10.1175/jamc-d-16-0161.1.

May, P. T., and J. M. Wilczak (1993), Diurnal and Seasonal-Variations of Boundary-Layer Structure Observed with a Radar Wind Profiler and Rass, *Monthly Weather Review*, *121*(3), 673-682, doi:Doi 10.1175/1520-0493(1993)121<0673:Dasvob>2.0.Co;2.

McCauley, M. P., and A. P. Sturman (1999), A study of orographic blocking and barrier wind development upstream of the Southern Alps, New Zealand, *Meteorol Atmos Phys*, *70*(3-4), 121-131, doi:DOI 10.1007/s007030050029.

McPherson, R. A. (2007), A review of vegetation-atmosphere interactions and their influences on mesoscale phenomena, *Prog Phys Geog*, *31*(3), 261-285, doi:10.1177/0309133307079055.

McPherson, R. A., and D. J. Stensrud (2005), Influences of a winter wheat belt on the evolution of the boundary layer, *Monthly Weather Review*, *133*(8), 2178-2199, doi:Doi 10.1175/Mwr2968.1.

McPherson, R. A., D. J. Stensrud, and K. C. Crawford (2004), The impact of Oklahoma's winter wheat belt on the mesoscale environment, *Monthly Weather Review*, *132*(2), 405-421, doi:Doi 10.1175/1520-0493(2004)132<0405:Tiooww>2.0.Co;2.

Mearns, L. O., et al. (2012), THE NORTH AMERICAN REGIONAL CLIMATE CHANGE ASSESSMENT PROGRAM Overview of Phase I Results, *B Am Meteorol Soc*, *93*(9), 1337-1362.

Medina, S., B. F. Smull, R. A. Houze, and M. Steiner (2005), Cross-barrier flow during orographic precipitation events: Results from MAP and IMPROVE, *J Atmos Sci*, *62*(10), 3580-3598, doi:Doi 10.1175/Jas3554.1.

Miao, Y., X.-M. Hu, S. Liu, T. Qian, M. Xue, Y. Zheng, and S. Wang (2015), Seasonal variation of local atmospheric circulations and boundary layer structure in the Beijing-Tianjin-Hebei region and implications for air quality, *Journal of Advances in Modeling Earth Systems*, *7*(4), 1602-1626, doi:10.1002/2015ms000522.

Miguez-Macho, G., G. L. Stenchikov, and A. Robock (2004), Spectral nudging to eliminate the effects of domain position and geometry in regional climate model simulations, *J Geophys Res-Atmos*, *109*(D13), doi:D13104, 10.1029/2003jd004495.

Miller, D. A., and R. A. White (1998), A Conterminous United States Multilayer Soil Characteristics Dataset for Regional Climate and Hydrology Modeling, *Earth Interactions*, *2*(2), 1-26, doi:10.1175/1087-3562(1998)002<0001:acusms>2.3.co;2.

Miller, S. T. K., B. D. Keim, R. W. Talbot, and H. Mao (2003), Sea breeze: Structure, forecasting, and impacts, *Rev Geophys*, *41*(3), doi:1011, Doi 10.1029/2003rg000124.

Mlawer, E. J., S. J. Taubman, P. D. Brown, M. J. Iacono, and S. A. Clough (1997), Radiative transfer for inhomogeneous atmospheres: RRTM, a validated correlated-k model for the longwave, *J Geophys Res-Atmos*, *102*(D14), 16663-16682, doi:Doi 10.1029/97jd00237.

Morrison, H., G. Thompson, and V. Tatarskii (2009), Impact of Cloud Microphysics on the Development of Trailing Stratiform Precipitation in a Simulated Squall Line: Comparison of One- and Two-Moment Schemes, *Monthly Weather Review*, *137*(3), 991-1007, doi:10.1175/2008mwr2556.1.

Nelson, B. R., O. P. Prat, D. J. Seo, and E. Habib (2016), Assessment and Implications of NCEP Stage IV Quantitative Precipitation Estimates for Product Intercomparisons, *Weather Forecast*, *31*(2), 371-394, doi:10.1175/Waf-D-14-00112.1.

Nielsen, E. R., R. S. Schumacher, and A. M. Keclik (2016), The Effect of the Balcones Escarpment on Three Cases of Extreme Precipitation in Central Texas, *Monthly Weather Review*, *144*(1), 119-138, doi:10.1175/MWR-D-15-0156.1.

Ookouchi, Y., M. Segal, R. C. Kessler, and R. A. Pielke (1984), Evaluation of Soil-Moisture Effects on the Generation and Modification of Mesoscale Circulations, *Monthly Weather Review*, *112*(11), 2281-2292, doi:Doi 10.1175/1520-0493(1984)112<2281:Eosmeo>2.0.Co;2.

Pan, F. F., and R. B. Smith (1999), Gap winds and wakes: SAR observations and numerical simulations, *J Atmos Sci*, *56*(7), 905-923, doi:Doi 10.1175/1520-0469(1999)056<0905:Gwawso>2.0.Co;2.

Pardyjak, E. R., H. J. S. Fernando, J. C. R. Hunt, A. A. Grachev, and J. Anderson (2009), A case study of the development of nocturnal slope flows in a wide open valley and associated air quality implications, *Meteorol Z*, *18*(1), 85-100, doi:10.1127/0941-2948/2009/362.

Parish, T. R. (1982), Barrier Winds Along the Sierra-Nevada Mountains, *J Appl Meteorol*, *21*(7), 925-930, doi:Doi 10.1175/1520-0450(1982)021<0925:Bwatsn>2.0.Co;2.

Paul, S., S. Ghosh, R. Oglesby, A. Pathak, A. Chandrasekharan, and R. A. A. J. Ramsankaran (2016), Weakening of Indian Summer Monsoon Rainfall due to Changes in Land Use Land Cover, *Sci Rep-Uk*, *6*, doi:32177, 10.1038/srep32177.

Pedgley, D. E. (1970), HEAVY RAINFALLS OVER SNOWDONIA, *Weather*, *25*(8), 340-350, doi:10.1002/j.1477-8696.1970.tb04117.x.

Petkovic, V., and C. D. Kummerow (2012), A Spatiotemporal Correlation Technique to Improve Satellite Rainfall Accumulation, *J Appl Meteorol Clim*, *51*(12), 2122-2136, doi:10.1175/Jamc-D-11-0178.1.

Pierrehumbert, R. T., and B. Wyman (1985), Upstream Effects of Mesoscale Mountains, *J Atmos Sci*, *42*(10), 977-1003, doi:Doi 10.1175/1520-0469(1985)042<0977:Ueomm>2.0.Co;2.

Porson, A., D. G. Steyn, and G. Schayes (2007), Formulation of an index for sea breezes in opposing winds, *J Appl Meteorol Clim*, *46*(8), 1257-1263, doi:Doi 10.1175/Jam2525.1.

Prein, A. F., R. M. Rasmussen, K. Ikeda, C. Liu, M. P. Clark, and G. J. Holland (2017), The future intensification of hourly precipitation extremes, *Nature Clim. Change*, *7*(1), 48-52, doi:10.1038/nclimate3168, http://www.nature.com/nclimate/journal/v7/n1/abs/nclimate3168.html - supplementary-information.

Qiao, F. X., and X. Z. Liang (2015), Effects of cumulus parameterizations on predictions of summer flood in the Central United States, *Clim Dynam*, *45*(3-4), 727-744, doi:10.1007/s00382-014-2301-7.

Reinecke, P. A., and D. Durran (2009), The Overamplification of Gravity Waves in Numerical Solutions to Flow over Topography, *Monthly Weather Review*, *137*(5), 1533-1549, doi:10.1175/2008mwr2630.1.

Rendon, A. M., J. F. Salazar, C. A. Palacio, and V. Wirth (2015), Temperature Inversion Breakup with Impacts on Air Quality in Urban Valleys Influenced by Topographic Shading, *J Appl Meteorol Clim*, *54*(2), 302-321, doi:10.1175/Jamc-D-14-0111.1.

Rotach, M. W., and D. Zardi (2007), On the houndary-layer structure over highly complex terrain: Key findings from MAP, *Q J Roy Meteor Soc*, *133*(625), 937-948, doi:10.1002/qj.71.

Rotunno, R., and R. Ferretti (2001), Mechanisms of intense alpine rainfall, *J Atmos Sci*, *58*(13), 1732-1749, doi:Doi 10.1175/1520-0469(2001)058<1732:Moiar>2.0.Co;2.

Saharia, M., P.-E. Kirstetter, H. Vergara, J. J. Gourley, Y. Hong, and M. Giroud (2017), Mapping Flash Flood Severity in the United States, *J Hydrometeorol*, *18*(2), 397-411, doi:10.1175/jhm-d-16-0082.1.

Schadler, G. (1990), Triggering of Atmospheric Circulations by Moisture Inhomogeneities of the Earths Surface, *Boundary-Layer Meteorology*, *51*(1-2), 1-29, doi:Doi 10.1007/Bf00120459.

Schwerdtfeger, W. (1979), Meteorological Aspects of the Drift of Ice from the Weddell Sea toward the Mid-Latitude Westerlies, *J Geophys Res-Oc Atm*, *84*(Nc10), 6321-6328, doi:Doi 10.1029/Jc084ic10p06321.

Segal, M., and R. W. Arritt (1992), Nonclassical Mesoscale Circulations Caused by Surface Sensible Heat-Flux Gradients, *B Am Meteorol Soc*, *73*(10), 1593-1604, doi:Doi 10.1175/1520-0477(1992)073<1593:Nmccbs>2.0.Co;2.

Serafin, S., L. Strauss, and V. Grubišić (2017), Climatology of Westerly Wind Events in the Lee of the Sierra Nevada, *J Appl Meteorol Clim*, *56*(4), 1003-1023, doi:10.1175/jamc-d-16-0244.1.

Shafter, M., D. Ojima, J. M. Antle, D. Kluck, R. McPherson, S. Petersen, B. Scanlon, and K. Sherman (2014), Ch. 19: Great Plains, in *Climate Change Impacts in the United States: The Third National Climate Assessment*, edited by J. M. Melillo, T. Richmond and G. W. Yohe, pp. 441-461, U.S. Global Change Research Program, doi:10.7930/J0D798BC.

Sheridan, P. F., V. Horlacher, G. G. Rooney, P. Hignett, S. D. Mobbs, and S. B. Vosper (2007), Influence of lee waves on the near-surface flow downwind of the Pennines, *Q J Roy Meteor Soc*, *133*(627), 1353-1369, doi:Doi 10.1002/Qj.110.

Skamarock, W. C., and Coauthors (2008), A description of the advanced research WRF version 3. NCAR Tech. Note TN-475_STR, edited, p. 113.

Smith, R. B. (1982), Synoptic Observations and Theory of Orographically Disturbed Wind and Pressure, *J Atmos Sci*, *39*(1), 60-70, doi:Doi 10.1175/1520-0469(1982)039<0060:Soatoo>2.0.Co;2.

Smith, S. A. (2004), Observations and simulations of the 8 November 1999 MAP mountain wave case, *Q J Roy Meteor Soc*, *130*(599), 1305-1325, doi:10.1256/qj.03.112.

Spero, T. L., M. J. Otte, J. H. Bowden, and C. G. Nolte (2014), Improving the representation of clouds, radiation, and precipitation using spectral nudging in the Weather Research and Forecasting model, *J Geophys Res-Atmos*, *119*(20), 11682-11694, doi:10.1002/2014jd022173.

Steele, C. J., S. R. Dorling, R. von Glasow, and J. Bacon (2013), Idealized WRF model sensitivity simulations of sea breeze types and their effects on offshore windfields, *Atmos Chem Phys*, *13*(1), 443-461, doi:DOI 10.5194/acp-13-443-2013.

Steele, C. J., S. R. Dorling, R. von Glasow, and J. Bacon (2015), Modelling sea-breeze climatologies and interactions on coasts in the southern North Sea: implications for offshore wind energy, *Q J Roy Meteor Soc*, *141*(690), 1821-1835, doi:10.1002/qj.2484.

Steiner, J. L., P. J. Starks, J. D. Garbrecht, D. N. Moriasi, X. C. Zhang, J. M. Schneider, J. A. Guzman, and E. Osei (2014), Long-Term Environmental Research: The Upper Washita River Experimental Watersheds, Oklahoma, USA, *J Environ Qual*, *43*(4), 1227-1238, doi:10.2134/jeq2014.05.0229.

Steyn, D., S. J. De Wekker, M. Kossmann, and A. Martilli (2013), Boundary Layers and Air Quality in Mountainous Terrain, in *Mountain Weather Research and Forecasting*, edited by F. K. Chow, S. F. J. De Wekker and B. J. Snyder, pp. 261-289, Springer Netherlands, doi:10.1007/978-94-007-4098-3_5.

Sun, J. H., and F. Q. Zhang (2012), Impacts of Mountain-Plains Solenoid on Diurnal Variations of Rainfalls along the Mei-Yu Front over the East China Plains, *Monthly Weather Review*, *140*(2), 379-397, doi:10.1175/Mwr-D-11-00041.1.

Sun, W. Y., and Y. Ogura (1979), Boundary-Layer Forcing as a Possible Trigger to a Squall-Line Formation, *J Atmos Sci*, *36*(2), 235-254, doi:Doi 10.1175/1520-0469(1979)036<0235:Blfaap>2.0.Co;2.

Sun, W. Y., and C. C. Wu (1992), Formation and Diurnal-Variation of the Dryline, *J Atmos Sci*, *49*(17), 1606-1619, doi:Doi 10.1175/1520-0469(1992)049<1606:Fadvot>2.0.Co;2.

Sun, X., M. Xue, J. Brotzge, R. A. McPherson, X.-M. Hu, and X.-Q. Yang (2016), An evaluation of dynamical downscaling of Central Plains summer precipitation using a WRF-based regional climate model at a convection-permitting 4 km resolution, *Journal of Geophysical Research: Atmospheres*, n/a-n/a, doi:10.1002/2016JD024796.

Takane, Y., H. Kondo, H. Kusaka, J. Katagi, O. Nagafuchi, K. Nakazawa, N. Kaneyasu, and Y. Miyakami (2017), Foehnlike Wind with a Traditional Foehn Effect plus Dry-Diabatic Heating from the Ground Surface Contributing to High Temperatures at the End of a Leeward Area, *J Appl Meteorol Clim*, *56*(7), 2067-2079, doi:10.1175/Jamc-D-16-0257.1.

Taylor, C. M., R. A. M. de Jeu, F. Guichard, P. P. Harris, and W. A. Dorigo (2012), Afternoon rain more likely over drier soils, *Nature*, *489*(7416), 423-426, doi:10.1038/nature11377.

Tripathi, O. P., and F. Dominguez (2013), Effects of spatial resolution in the simulation of daily and subdaily precipitation in the southwestern US, *J Geophys Res-Atmos*, *118*(14), 7591-7605, doi:10.1002/jgrd.50590.

Tripoli, G. J., and W. R. Cotton (1989a), Numerical Study of an Observed Orogenic Mesoscale Convective System .1. Simulated Genesis and Comparison with Observations, *Monthly Weather Review*, *117*(2), 273-304, doi:Doi 10.1175/1520-0493(1989)117<0273:Nsoaoo>2.0.Co;2.

Tripoli, G. J., and W. R. Cotton (1989b), Numerical Study of an Observed Orogenic Mesoscale Convective System .2. Analysis of Governing Dynamics, *Monthly Weather Review*, *117*(2), 305-328, doi:Doi 10.1175/1520-0493(1989)117<0305:Nsoaoo>2.0.Co;2.

von Storch, H., H. Langenberg, and F. Feser (2000), A spectral nudging technique for dynamical downscaling purposes, *Mon Weather Rev*, *128*(10), 3664-3673, doi:Doi 10.1175/1520-0493(2000)128<3664:Asntfd>2.0.Co;2.

Vosper, S. B., P. F. Sheridan, and A. R. Brown (2006), Flow separation and rotor formation beneath two-dimensional trapped lee waves, *Q J Roy Meteor Soc*, *132*(620), 2415-2438, doi:Doi 10.1256/Qj.05.174.

Wang, J. L., and V. R. Kotamarthi (2014), Downscaling with a nested regional climate model in near-surface fields over the contiguous United States, *J Geophys Res-Atmos*, *119*(14), 8778-8797, doi:10.1002/2014jd021696.

Wang, Q. W., M. Xue, and Z. M. Tan (2016), Convective initiation by topographically induced convergence forcing over the Dabie Mountains on 24 June 2010, *Adv Atmos Sci*, *33*(10), 1120-1136, doi:10.1007/s00376-016-6024-z.

Westra, S., H. J. Fowler, J. P. Evans, L. V. Alexander, P. Berg, F. Johnson, E. J. Kendon, G. Lenderink, and N. M. Roberts (2014), Future changes to the intensity and frequency of short-duration extreme rainfall, *Rev Geophys*, *52*(3), 522-555, doi:10.1002/2014rg000464.

Whiteman, C. D., and J. C. Doran (1993), The Relationship between Overlying Synoptic-Scale Flows and Winds within a Valley, *J Appl Meteorol*, *32*(11), 1669-1682, doi:Doi 10.1175/1520-0450(1993)032<1669:Trboss>2.0.Co;2.

Wolyn, P. G., and T. B. Mckee (1994), The Mountain Plains Circulation East of a 2-Km-High North South Barrier, *Monthly Weather Review*, *122*(7), 1490-1508, doi:Doi 10.1175/1520-0493(1994)122<1490:Tmpceo>2.0.Co;2.

Xu, Q. (1990), A theoretical study of cold-air damming, *J. Atmos. Sci.*, *47*, 2969-2985.

Yan, H., and R. A. Anthes (1988), The Effect of Variations in Surface Moisture on Mesoscale Circulations, *Monthly Weather Review*, *116*(1), 192-208, doi:Doi 10.1175/1520-0493(1988)116<0192:Teovis>2.0.Co;2.

Yang, Y., and Y. L. Chen (2008), Effects of terrain heights and sizes on island-scale circulations and rainfall for the island of Hawaii during HaRP, *Monthly Weather Review*, *136*(1), 120-146, doi:Doi 10.1175/2007mwr1984.1.

Zaitchik, B. F., J. P. Evans, and R. B. Smith (2007), Regional impact of an elevated heat source: The Zagros Plateau of Iran, *J Climate*, *20*(16), 4133-4146, doi:Doi 10.1175/Jcli4248.1.

Zhang, X. D., J. X. He, J. Zhang, I. Polyakov, R. Gerdes, J. Inoue, and P. L. Wu (2013), Enhanced poleward moisture transport and amplified northern high-latitude wetting trend, *Nat Clim Change*, *3*(1), 47-51, doi:10.1038/Nclimate1631.

Zhang, Y. C., J. H. Sun, and S. M. Fu (2014), Impacts of diurnal variation of mountain-plain solenoid circulations on precipitation and vortices east of the Tibetan Plateau during the mei-yu season, *Adv Atmos Sci*, *31*(1), 139-153, doi:10.1007/s00376-013-2052-0.

Zhu, J. H., and X. Z. Liang (2013), Impacts of the Bermuda High on Regional Climate and Ozone over the United States, *J Climate*, *26*(3), 1018-1032, doi:10.1175/Jcli-D-12-00168.1.

Figure captions

Figure 1. (a) Terrain height in Texas and (b) climatological precipitation in August during 2002-2015 retrieved from the Stage IV data. The three main metropolitan areas located along the Balcones Escarpment, i.e., San Antonio, Austin, and Dallas-Fort Worth (DFW), are marked.

Figure 2. Map of model domains for dynamic downscaling, with 20–>4km grid spacing for the two nested domains respectively. The background color shows the terrain height.

Figure 3. Mean hourly precipitation frequency (in count month^{-1}) for August 2002-2015 (left) retrieved from the Stage IV data and (right) downscaled by WRF at (top) 0900, (middle) 1300, and (bottom) 1500 CST. Note that the cities of Oklahoma City, Dallas-Ft. Worth, Austin, and San Antonio are marked with black stars from north to south, respectively. The white dashed line beside the three Texas cities denotes the location of the escarpment.

Figure 4. Mean hourly precipitation rate (in mm day^{-1}) for August 2002-2015 (left) retrieved from the Stage IV data and (right) downscaled by WRF at (top) 0900 and (bottom) 1500 CST.

Figure 5. Time series of hourly precipitation rate (in mm day^{-1}) averaged over the Edwards Plateau domain marked by dashed lines in Fig. 4b.

Figure 6. Spatial distribution of (a) terrain height (in km), (b) precipitation frequency (in count month^{-1}), and (c) vertical velocity (in cm s^{-1}) in the middle of the boundary layer (600 m AGL) at 1500 CST.

Figure 7. Spatial distribution of (a) soil types, (b) latent heat flux (LH, in W m^{-2}), (c) sensible heat flux (HFX, in W m^{-2}), (d) soil moisture (SMOIS, in fraction) (e) wilting point soil moisture content (WLTSMC, in fraction), and (f) moisture availability parameter (β) at 1200 CST.

Figure 8. West-to-east cross sections of (a) vertical velocity (w, in cm s^{-1}) and (b) rain water mixing ratio (QRAIN, in mg kg^{-1}) through Dallas, Texas at 2100 UTC (1500 CST). The dominant soil types are shaded under the thick black line, which indicated the terrain surface. The clay-based soil types 9 and 12 are shaded in dark red-brown; sand-based types 1 and 3 are shaded in yellow. Wind vectors are overlaid on each plot. Note that vertical velocity is multiplied by 100 when plotting wind vectors. The longitudinal position of Dallas (–96.8˚) is marked by a black rectangle on the x-axis.

Figure 9. (top to bottom) soil types (ISLTYP), terrain heights (HGT) used in the 4 single-day sensitivity simulations (one column for each simulation) and the correspondingly predicted latent heat flux (LH), sensible heat flux (HFX), vertical velocity (W) in the middle of the boundary layer, surface wind speed (WSP), and differences between soil moisture and wilting point (SMOIS-WLTSMC) at 1500 CST on 7 August 2011.

Table 1: Configuration for the sensitivity simulations for 7 August 2011

#	Simulation	configuration
1	Control	as in Hu and Xue [2016]
2	Change ISLTYP	Change the soil type in most Texas to sandy loam (type 3), see Fig. 9h
3	Change SOILPARM.TBL	Switch the DRYSMC and WLTSMC* between clay-based soil types (9 and 12) and sand (1)
4	Change HGT	Remove the terrain in most Texas (Fig. 9w)

*DRYSMC: Dry soil moisture; WLTSMC: Wilting point soil moisture, see their values for different soil types in Table 2.

Table 2: Dominant Soil Categories in Texas and their properties*

Soil Category	Soil Description	DRYSMC	WLTSMC
1	Sand	0.01	0.01
3	Sandy Loam	0.047	0.047
9	Clay Loam	0.103	0.103
12	Clay	0.138	0.138

*DRYSMC: Dry-soil moisture threshold at which direct evaporation from top-soil layer ends [volumetric fraction]; WLTSMC: Soil moisture value at the wilting point [volumetric fraction]

Figure 1.

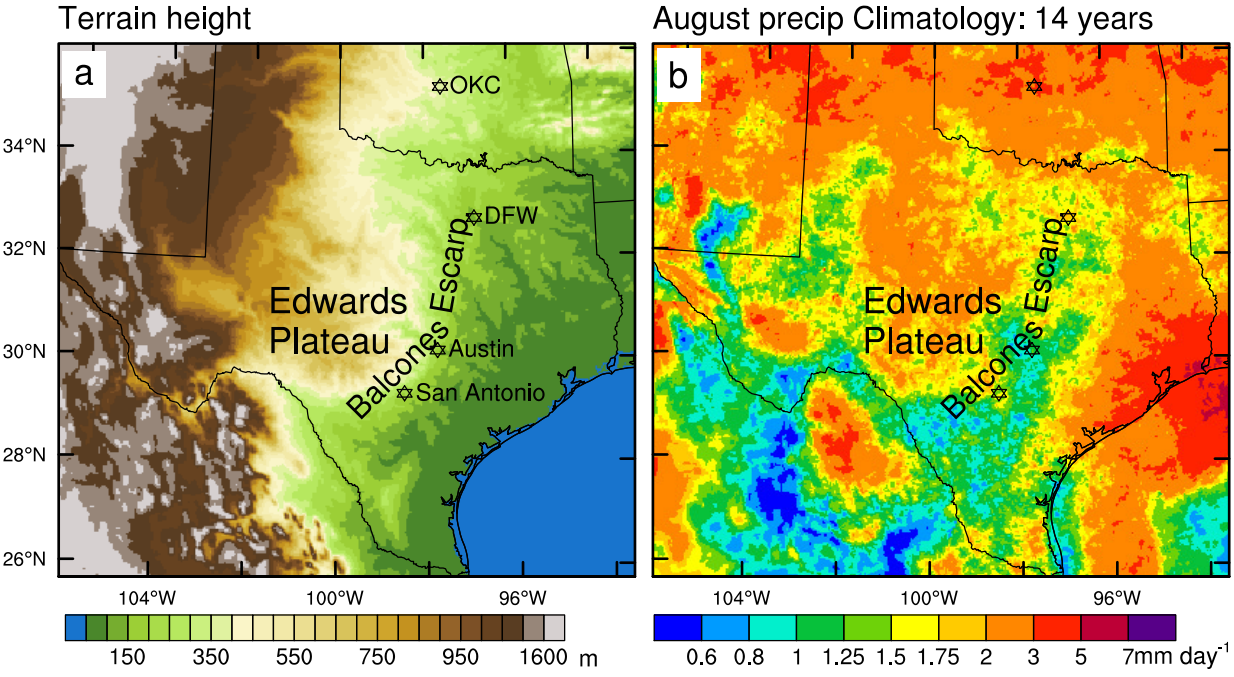
Terrain height
a
OKC
DFW
Edwards
Plateau
Balcones Escarp
Austin
San Antonio
34°N
32°N
30°N
28°N
26°N
104°W
100°W
96°W
150
350
550
750
950
1600
m
August precip Climatology: 14 years
b
Edwards
Plateau
Balcones Escarp
104°W
100°W
96°W
0.6
0.8
1
1.25
1.5
1.75
2
3
5
7mm day-1

Figure 2.

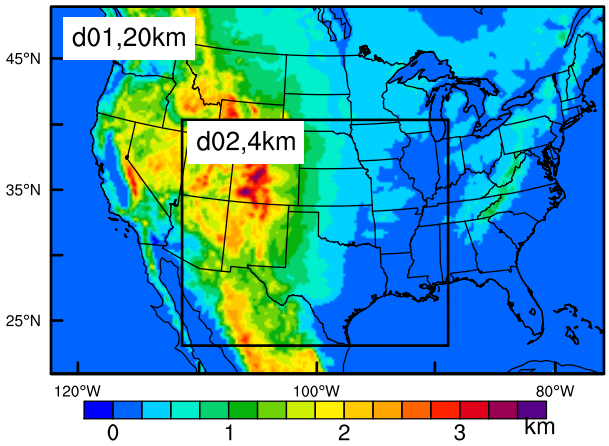
d01,20km
d02,4km
45°N
35°N
25°N
120°W
100°W
80°W
0
1
2
3
km

Figure 3.

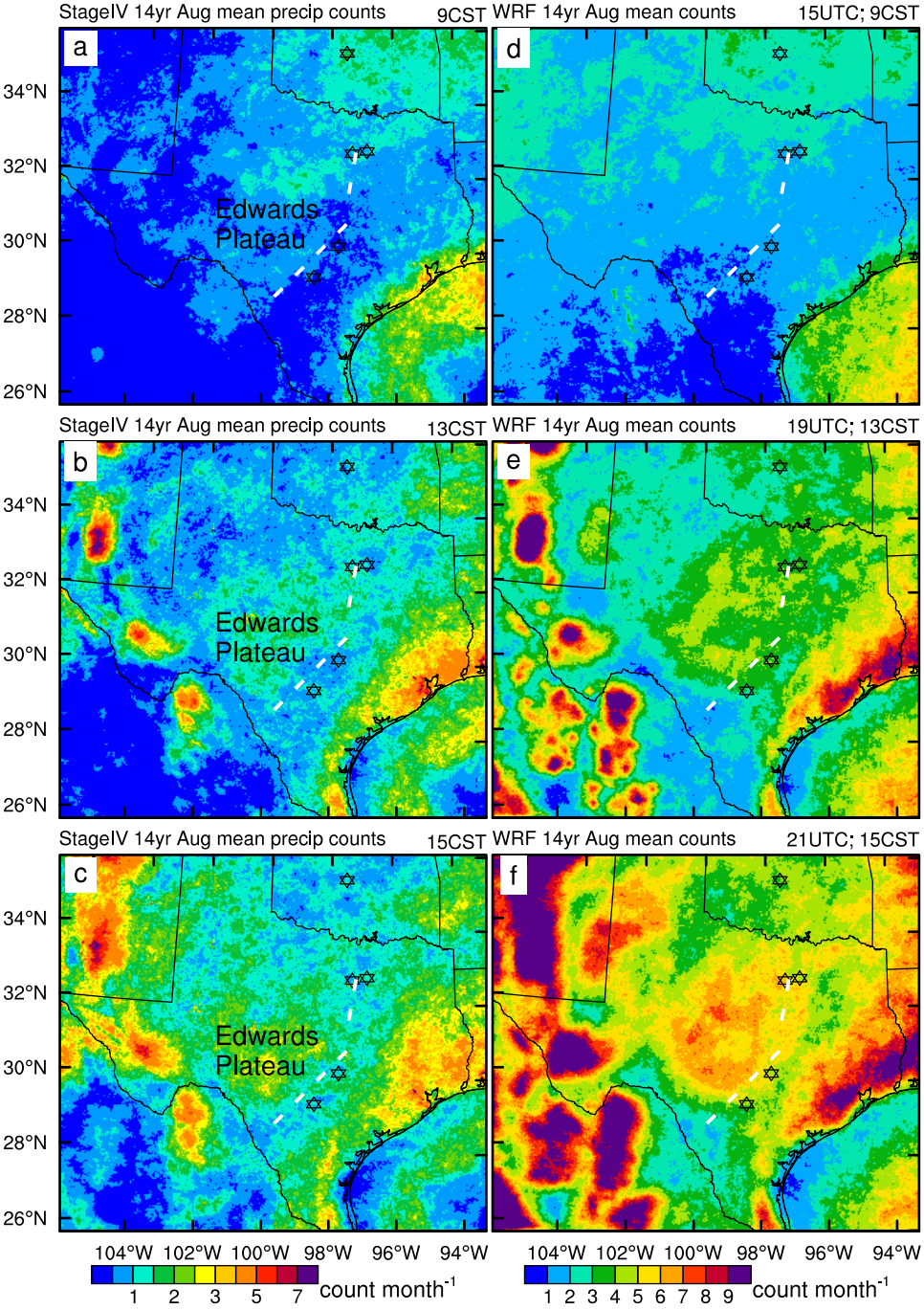
StageIV 14yr Aug mean precip counts
9CST
WRF 14yr Aug mean counts
15UTC; 9CST
a
d
Edwards Plateau
StageIV 14yr Aug mean precip counts
13CST
WRF 14yr Aug mean counts
19UTC; 13CST
b
e
Edwards Plateau
StageIV 14yr Aug mean precip counts
15CST
WRF 14yr Aug mean counts
21UTC; 15CST
c
f
Edwards Plateau
34°N
32°N
30°N
28°N
26°N
104°W 102°W 100°W 98°W 96°W 94°W
1 2 3 5 7
count month-1
1 2 3 4 5 6 7 8 9
count month-1

Figure 4.

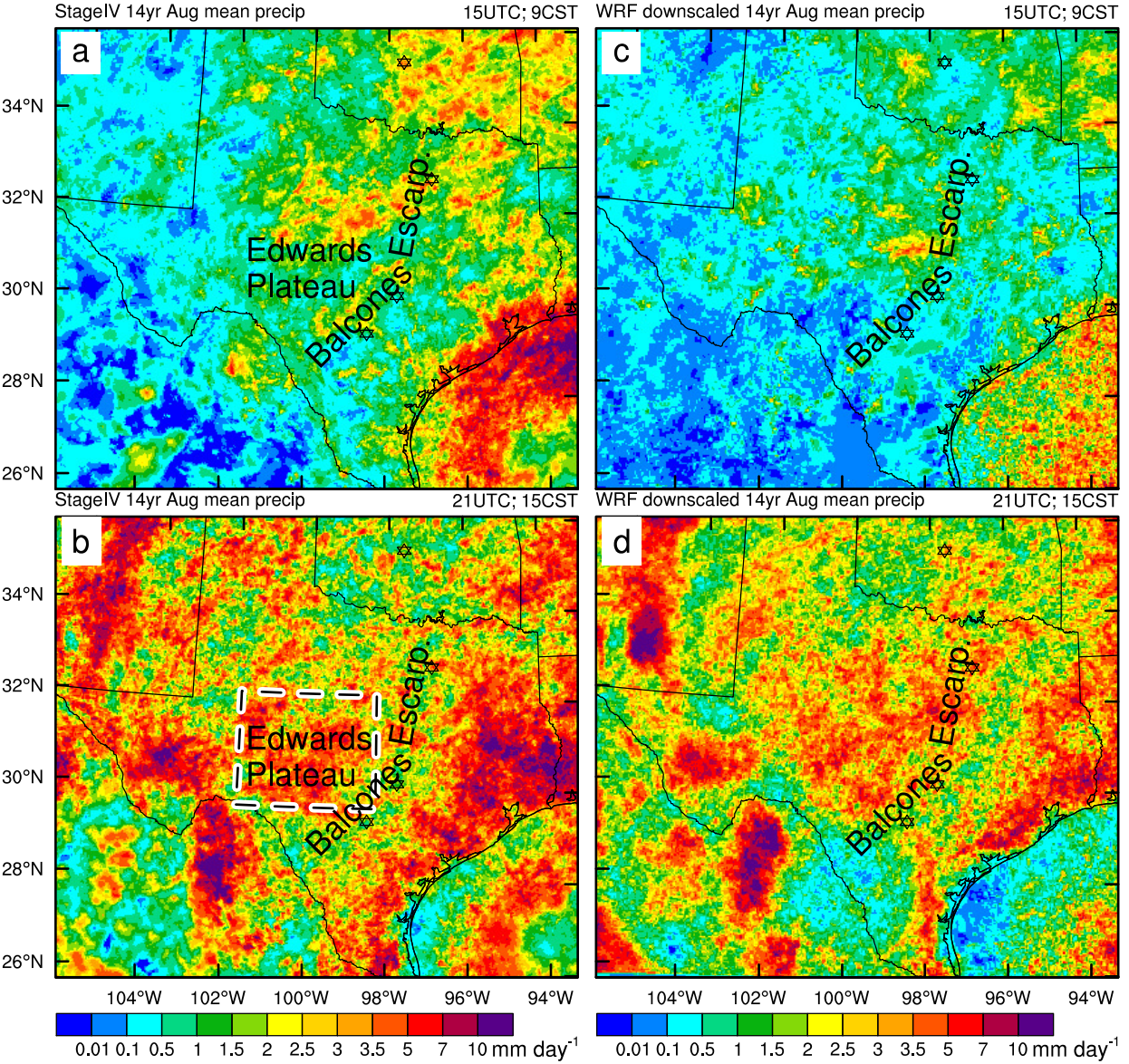
StageIV 14yr Aug mean precip
15UTC; 9CST
WRF downscaled 14yr Aug mean precip
15UTC; 9CST
StageIV 14yr Aug mean precip
21UTC; 15CST
WRF downscaled 14yr Aug mean precip
21UTC; 15CST
a
b
c
d
Edwards Plateau
Balcones Escarp.
34°N
32°N
30°N
28°N
26°N
104°W
102°W
100°W
98°W
96°W
94°W
0.01 0.1 0.5 1 1.5 2 2.5 3 3.5 5 7 10 mm day-1

Figure 5.

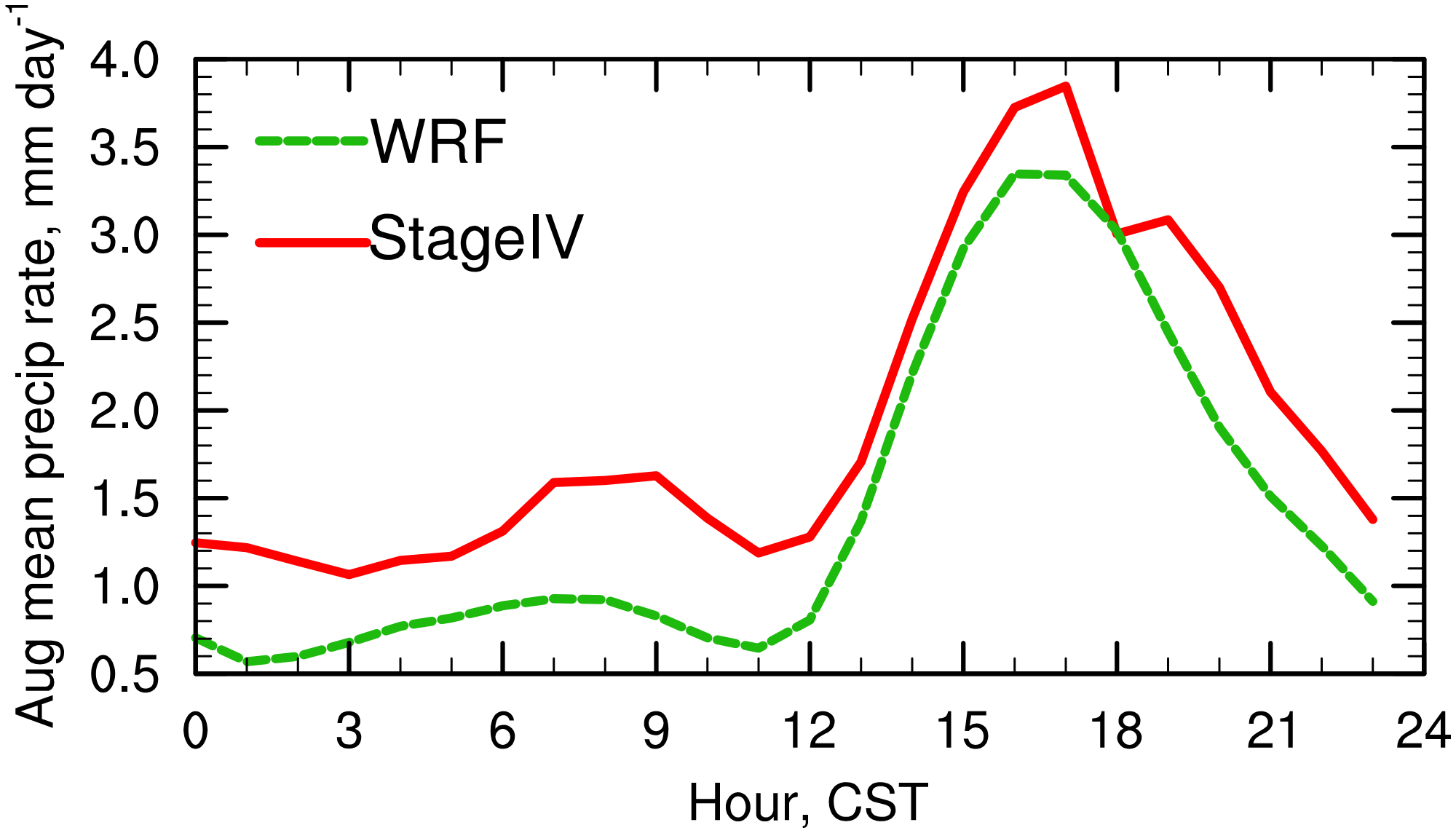
WRF
StageIV
Aug mean precip rate, mm day^{-1}
4.0
3.5
3.0
2.5
2.0
1.5
1.0
0.5
0
3
6
9
12
15
18
21
24
Hour, CST

Figure 6.

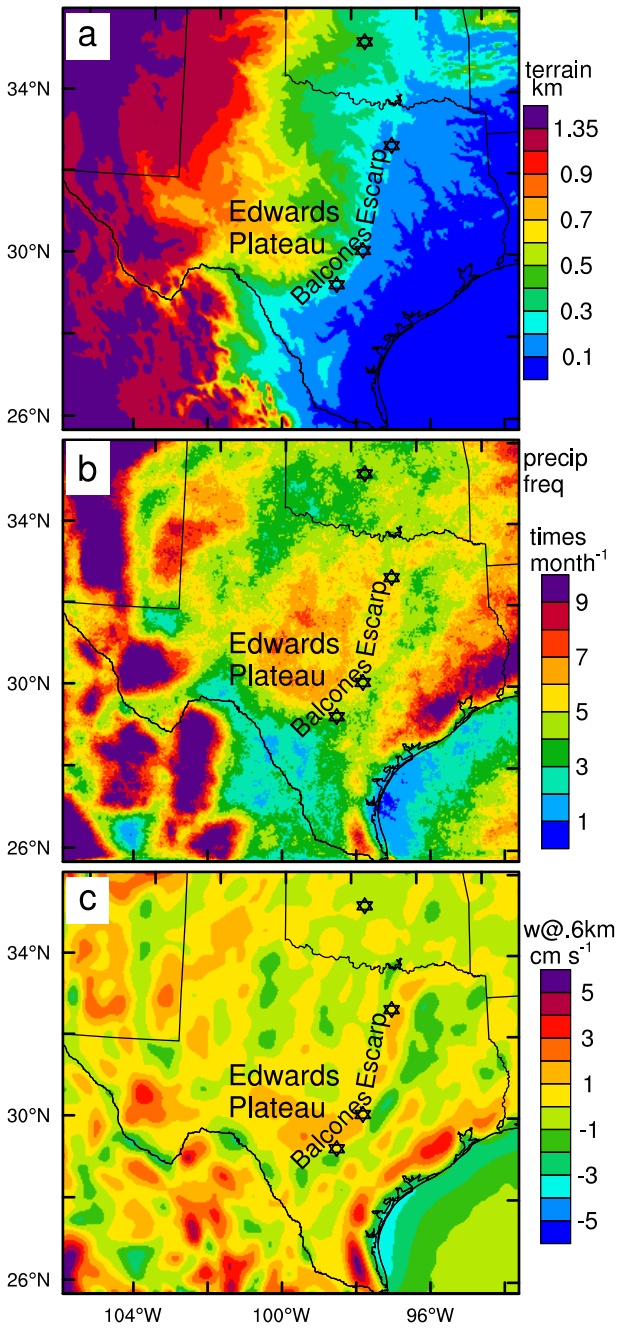
a
terrain
km
1.35
0.9
0.7
0.5
0.3
0.1
Edwards
Plateau
Balcones Escarp
34°N
30°N
26°N
b
precip
freq
times
month-1
9
7
5
3
1
c
w@.6km
cm s-1
5
3
1
-1
-3
-5
104°W
100°W
96°W

Figure 7.

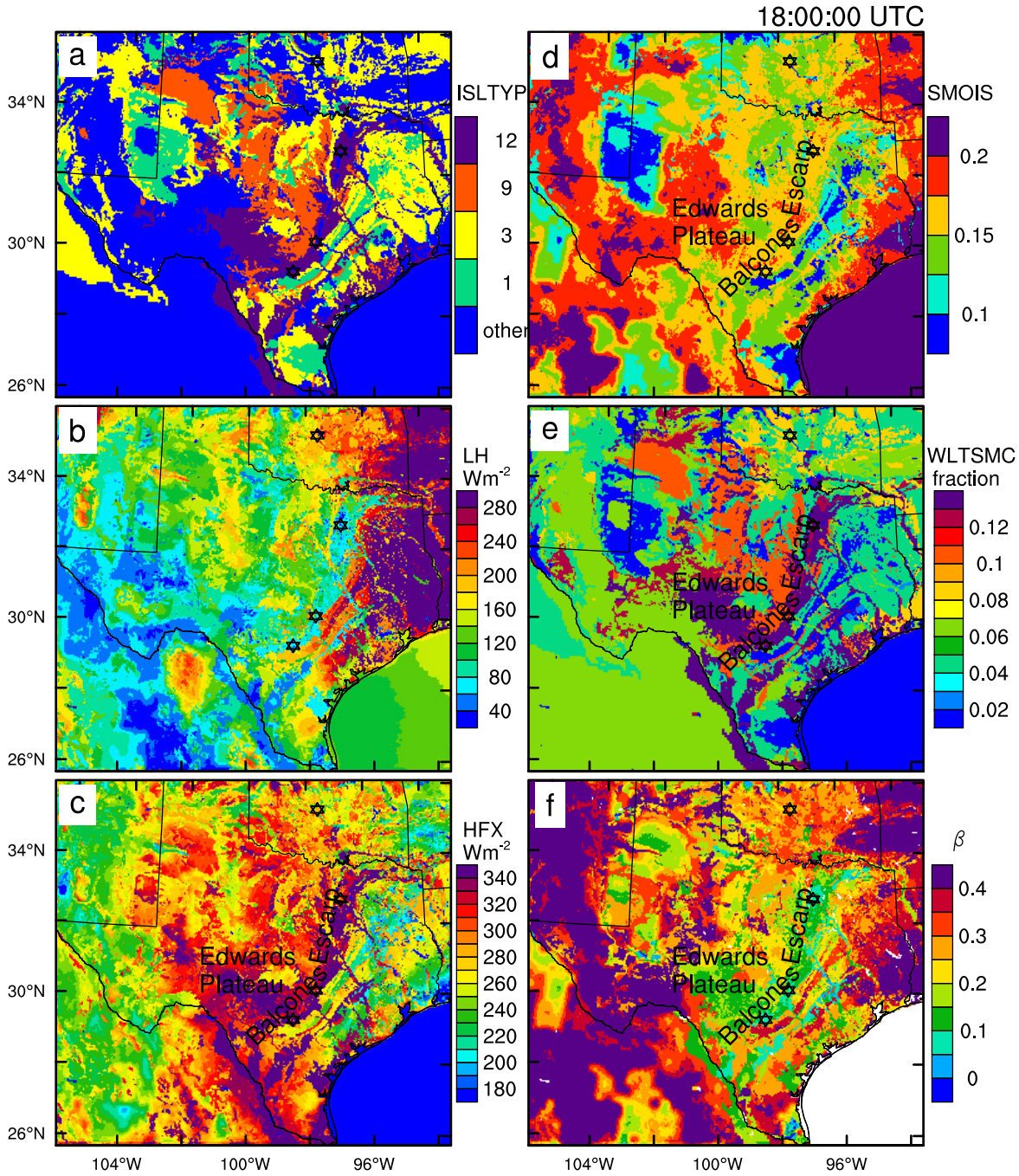
18:00:00 UTC
a
b
c
d
e
f
ISLTYP
12
9
3
1
other
SMOIS
0.2
0.15
0.1
LH
Wm-2
280
240
200
160
120
80
40
WLTSMC
fraction
0.12
0.1
0.08
0.06
0.04
0.02
HFX
Wm-2
340
320
300
280
260
240
220
200
180
β
0.4
0.3
0.2
0.1
0
Edwards
Plateau
Balcones Escarp
34°N
30°N
26°N
104°W
100°W
96°W

Figure 8.

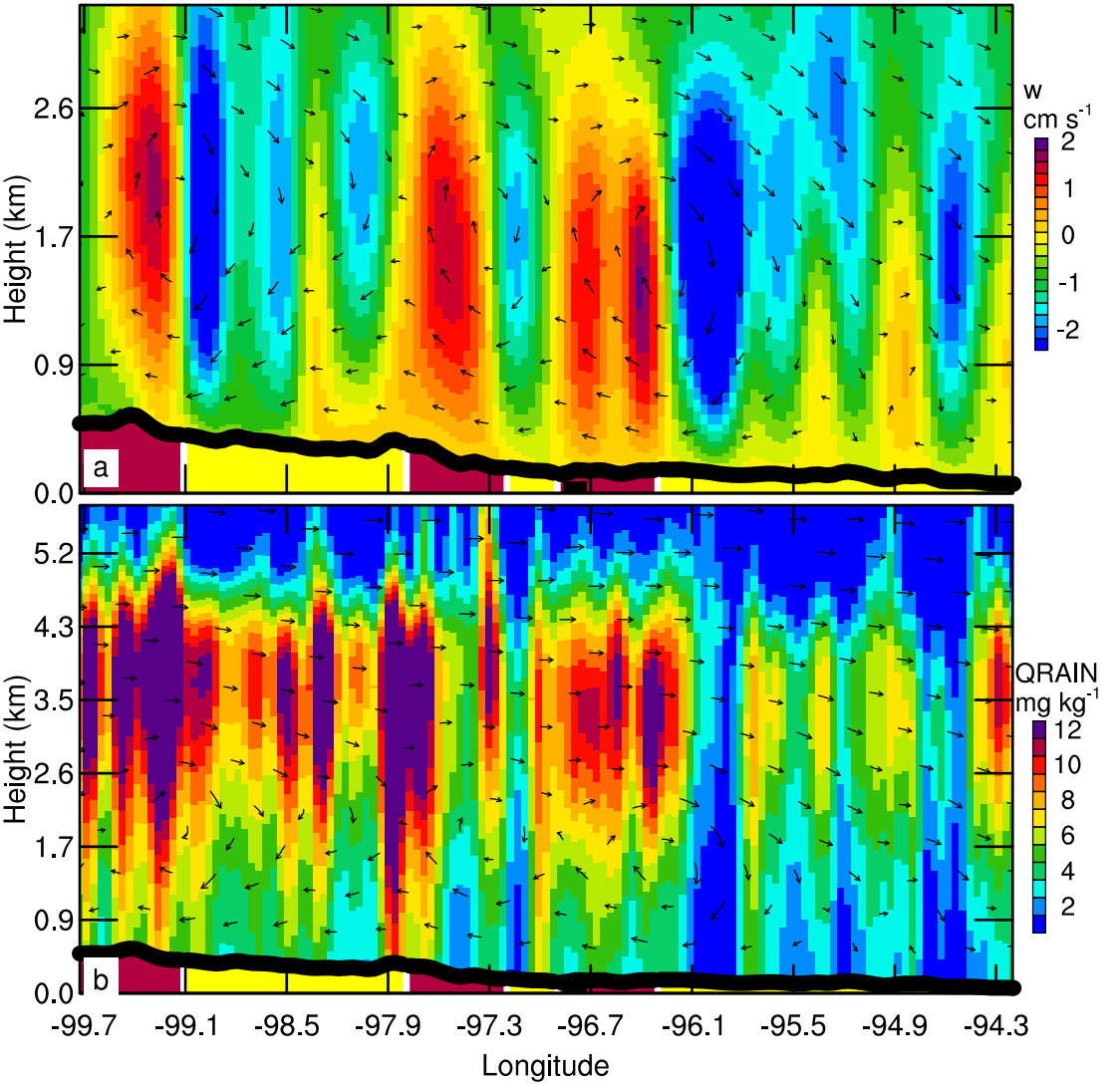
w
cm s-1
2
1
0
-1
-2
Height (km)
2.6
1.7
0.9
0.0
a
QRAIN
mg kg-1
12
10
8
6
4
2
5.2
4.3
3.5
b
-99.7
-99.1
-98.5
-97.9
-97.3
-96.7
-96.1
-95.5
-94.9
-94.3
Longitude

Figure 9.

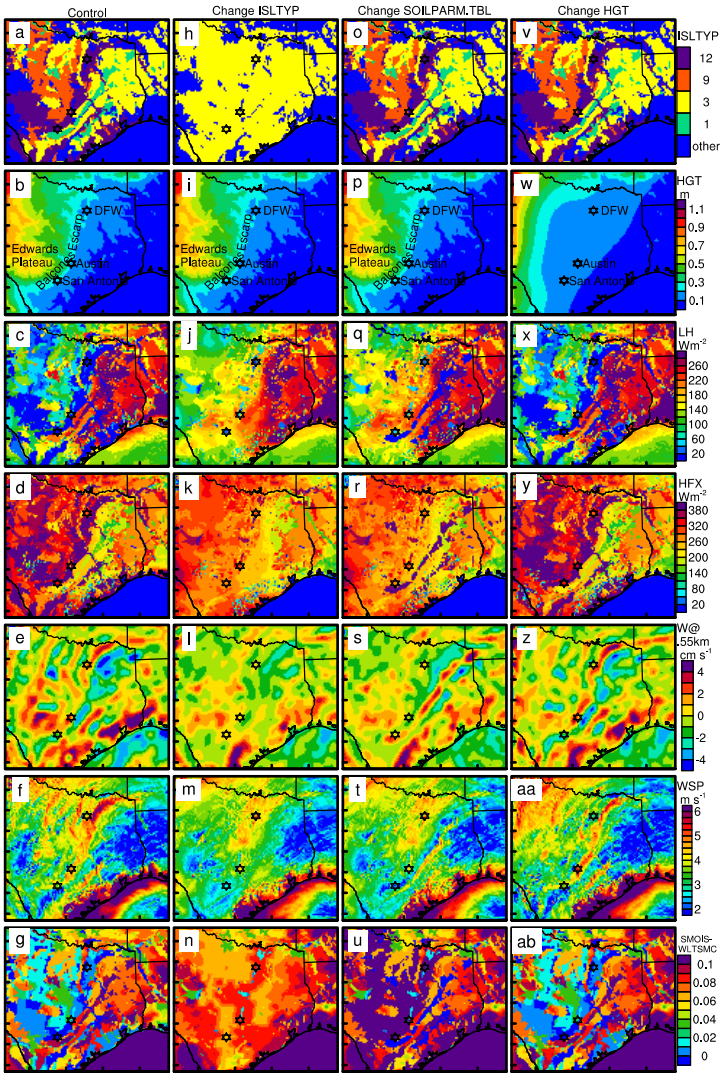
Control
Change ISLTYP
Change SOILPARM.TBL
Change HGT
a
h
o
v
ISLTYP
12
9
3
1
other
b
i
p
w
HGT
m
1.1
0.9
0.7
0.5
0.3
0.1
DFW
Edwards
Plateau
Balcones Escarp.
Austin
San Antonio
c
j
q
x
LH
Wm-2
260
220
180
140
100
60
20
d
k
r
y
HFX
Wm-2
380
320
260
200
140
80
20
e
l
s
z
W@
.55km
cm s-1
4
2
0
-2
-4
f
m
t
aa
WSP
m s-1
6
5
4
3
2
g
n
u
ab
SMOIS-
WLTSMC
0.1
0.08
0.06
0.04
0.02
0